How does Lithology Influence the Migration and Stability of Meandering Bedrock Rivers?

A Senior Thesis Presented to
the Faculty of the Department of Geology

Bachelor of Arts

Zhilin Shi
The Colorado College
May 2023

ACKNOWLEDGEMENTS

I would like to begin by expressing my deepest gratitude to Prof. Sarah Schanz, whose unwavering support made all of this possible. During my sophomore year, I enrolled in Geomorphology and was intrigued by the research opportunities that Sarah had mentioned. I contacted her, and she informed me that a research opportunity studying bedrock meandering rivers would be available to me in the summer of my junior year. I must admit, I didn't fully comprehend what a bedrock river was until I began the research in June of my rising senior year. It was a challenging process, and I struggled to grasp the concepts at times. Nevertheless, Sarah was always there to assist me whenever I faced difficulties. I am immensely grateful for her guidance and for shaping me into a promising future geologist.

I am also thankful to Prof. Brian Yanites, a faculty member of the Earth and Atmospheric Science Department at Indiana University Bloomington, for granting me access to utilize the supercomputer for running the model.

I am immensely grateful to the Geology Department at Colorado College for providing me with the opportunity to enroll in numerous geology courses. These courses have played a vital role in establish a strong foundation for my understanding of Earth's processes and history. Additionally, they have allowed me to expand my horizons and delve into various subfields within Earth Science, including geochronology, volcanology, sedimentology, geochemistry, and geomorphology.

Lastly, I would like to express my heartfelt appreciation to my parents for their financial assistance, which made it possible for me to travel to the United States and pursue a career in Earth Science. Their generosity and flexibility have afforded me the opportunity to follow my dreams and pursue my passion. I am deeply grateful for their steadfast support.

TABLE OF CONTENTS

ABSTRACT 1

LITERATURE BACKGROUND 3

How do Meandering Bedrock Rivers Migrate? 3

The Stability Problem of Bedrock Meandering Rivers 4

The Role of Lithology in Bedrock River Erosion 6

STUDY AREA BACKGROUND 15

Smith River 15

Physical Features 15

Geology 16

Climate 17

Land-Use History 18

METHODS 20

Lateral Erodibility and Vertical Erodibility (*kl* & *kf*) 20

Initial Slope 21

Channel Type 22

Expected Model Output 22

Numerical Model 23

Channel Migration and Meandering 24

RESULT 26

Lateral Erodibility (*kl*) 26

General Trends 26

Exceptions 27

Vertical Erodibility (kf) 38

General Trends 38

Exceptions 39

Initial Slope 44

General Trends 44

Channel Geometry 46

General Trends 46

Lithologic Anisotropy 52

General Trends 52

Exceptions 53

DISCUSSION 58

Initial Slope 58

Channel Geometry 60

Erodibility ····· **61**
Lithologic Anisotropy ····· **63**
Smith River ····· **65**

CONCLUSION ····· **67**
REFERENCE ····· **69**

ABSTRACT

Bedrock meandering rivers are widely distributed over the planet. These rivers have little to no layered alluvium, and instead have episodically exposed bedrock as the banks and bed. Due to lack of a thick sediment cover, bedrock meandering river channels are sensitive to climatic and tectonic changes that are directly interacting with the channel either by inducing flooding, altering sediment supply, and/or uplifting of the channel (Stark et al., 2010; Finnegan & Balco, 2013). This unique characteristic makes bedrock meandering rivers actively incise and reshape the Earth's landscape. How fast the bedrock river channel migrates or erodes is strongly dependent on the substrate of the bedrock river (Sklar & Dietrich, 2004); therefore, lithology is hypothesized to be a strong control on the landscape evolution of bedrock meandering rivers.

The goal of this study is to explore the lithologic control on bedrock meandering rivers using a 1-D numerical model built by Drs. Sarah Schanz and Brian Yanites. Lithologic controls on the stability of meandering bedrock rivers – lateral erodibility, vertical erodibility, bedrock channel types, and initial slope – are varied in the models, which run for 100,000 model years to simulate distinct landscape evolution patterns. The patterns are then compared with real-world river channels, namely the Smith River, Oregon, USA. The similarities and differences between the simulated river channel patterns and actual channel trends provide insight into the role of lithologic strength on the migration and stability of meandering bedrock rivers, and the evolution of mountainous landscapes.

A single thread meandering bedrock river can evolve into a straight channel, meandering channel, or braided channel, depending on the balance between lateral and vertical erosion rates

and channel geometry. The behavior of the model is supported by direct field evidence from the Smith River.

LITERATURE BACKGROUND

How do Meandering Bedrock Rivers Migrate?

River channel planforms influence the style and tempo of topographic development, as well as the biodiversity and ecological potential. For instance, the degradation of a river channel can result in a lowering of the water table and changes in the surrounding plant life, leading to a shift from wetland and meadow habitats to drier shrublands. This further harms biodiversity and ecological balances. Species, such as beavers, greatly rely on healthy riparian ecosystem, and the changes in vegetation can lead to a lack of sufficient food and building material, potentially forcing them to relocate to other suitable habitats.

Bedrock meandering rivers are ubiquitous on Earth. However, many questions still remain vague for the scientific community, for example, how do bedrock rivers meander? Meandering rivers are single-thread and sinuous channels that have a relatively high sinuosity (>1.5) compared with braided channels, which are multiple-threaded and straight. Meandering channels are more common than braided channels on Earth, where meandering channels can be easily recognized in many geologic settings such as fluvial rivers, tidal flows, and submarine environments (Hooke, 2013). Meandering rivers migrate their channels through secondary flows that are perpendicular to the direction of primary flows, resulting in the accumulation of sediment and undercuts, respectively, at the inner bends and outer bends of meander loops (Fig. 1) (Seminara, 2006). The initiation of point bars and cut banks makes the channel more migratory because secondary flows drive an additional contribution to sediment transport and further modify the bed topography (Seminara, 2006).

Understanding river meandering and the variability in characteristics and processes helps scientists address many major questions. Ecology and biodiversity, including a range of types of habitats, are closely connected with meandering rivers, and their sensitivity directly reflects environmental change and response, acting as a key element to the change of the global environment (Hooke, 2013). Despite the importance of meandering bedrock rivers linked with many aspects of nature, prior research on meandering river dynamics and ecology focused on alluvial channels but largely ignoring bedrock rivers. This has resulted in a lack of knowledge regarding rates and processes of lateral migration in bedrock rivers. Accordingly, more scrutiny of bedrock meandering rivers is needed. For example, improved understanding of bedrock river meandering requires more quantification of the role of variables such as dynamic width, lithology, tectonics, climate, and the establishment of mathematical models to predict channel migration.

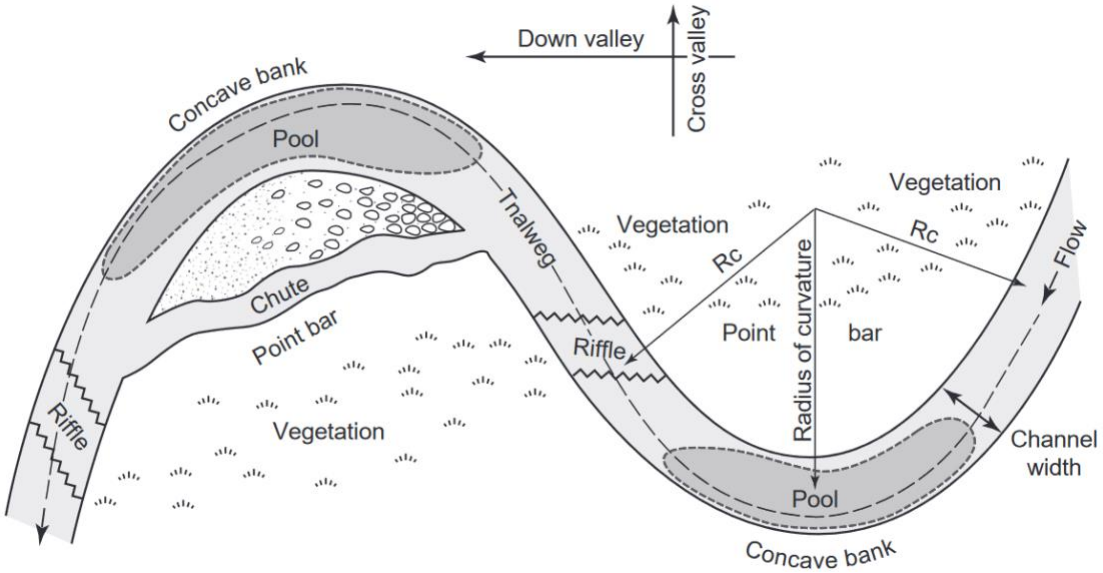

Figure 1. Common features of meanders (Hooke, 2013).

The Stability Problem of Bedrock Meandering Rivers

Bedrock meandering rivers tend to be supply-limited and so deviate from alluvial meandering rivers, which are transport-limited. Sediment in bedrock channels does not stay long before being transported downstream; therefore, sediment has little control in shaping the river planform (Wohl, 2015). Erosion and transport dominate the entire river ecosystem. Though alluvial river channels might experience more erosion than bedrock river channels, the large influx of sediment allows alluvial channels to create a thick layer that prevents direct contact between the bedrock substrate and the water, further facilitating ecosystem productivity (Wohl, 2015).

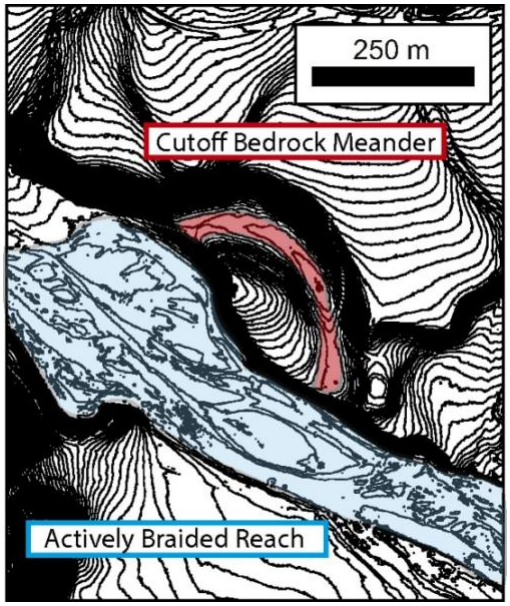

Figure 2. A braided section of the active channel next to an abandoned bedrock meander cutoff in Arroyo Seco, California, USA (Finnegan and Balco, 2013).

The lack of long-lasting sediment theoretically creates a negative feedback in meandering bedrock channels, although field evidence suggests this feedback is not always present. As the sinuosity of a meandering bedrock river increases, the channel width increases correspondingly because erosion of the outer bank is not matched by deposition on the inner bank, as occurs in

alluvial rivers (Mason and Mohrig, 2019). Rather, the inner bank remains stationary while water flow erodes and widens the outer bank; eventually, the channel cannot hold the water in a single channel, resulting in a wide, braided planform (Fig. 2) (Finnegan and Balco, 2013). This is directly opposed to an alluvial channel for which cut bank erosion is balanced by point bar deposition. Nonetheless, some bedrock rivers persist in meander planforms. For instance, the Yakima River, WA, preserves a long history of meander planforms throughout ~600 m incision into the Columbia Plateau, which was caused by differential uplift of the Manastash Ridge, Umtanum Ridge, and Selah Butte anticlines (Bender et al., 2016).

To a certain extent, changes in sediment supply, discharge, and water depth due to tectonics (Yanites et al., 2010), climate (Stark et al., 2010), lithology (Johnson and Finnegan, 2015), or any combination of these forces, might result in disturbance of the stability of meandering bedrock rivers and alter river planforms permanently. In order to parse out the influence of these forces, bedrock meandering can be broken down into two processes: lateral channel migration and vertical incision. The former widens the channel, transforming a single-thread meandering bedrock river into a multi-thread braided river (Finnegan and Balco, 2013). As a result, the water flows less vigorously through the channel. Vertical incision of bedrock makes the channel narrower. The old channels are abandoned as step-like landforms called strath terraces (Pazzaglia, 2013), which provide past evidence for relative lateral and vertical erosion rates. The balance of lateral migration and vertical incision can create long-lasting bedrock meanders by entrenching channel bends and preventing scour on the sediment-absent point bars. This balance is highly dependent on the lithologic strength, which dictates lateral versus vertical erosion susceptibility.

The Role of Lithology in Bedrock River Erosion

Tectonics, climates, and lithology all potentially play a role in disturbing the stability of bedrock meandering rivers by either driving channel widening or narrowing. The lithologic control on active bedrock meandering river channels is the primary focus of this study. Lithology, set as an intrinsic property, influences the erosion styles by which bedrock channels evolve (Fig. 3). Researchers have studied different types of bedrocks in field and laboratory settings in an attempt to unravel the connection between lithology and erodibility of bedrock rivers (Allen et al., 2013; Johnson and Finnegan, 2015; Bursztyn et al., 2015; Inoue et al., 2017).

Bursztyn et al. (2015) studied a fluvial transect of the Colorado Plateau where it approximately ranges from the Green River Basin, Wyoming, to the Grand Canyon, Arizona. They divided this transect into forty-nine distinct bedrock reaches and employed the Brazilian splitting test to measure tensile strength, as well as a Schmidt hammer, to measure compressive strength. Their findings suggest that except for erosion-resistant Quaternary igneous basalt and limestone, rock strength is dependent on rock type and its burial age (Fig. 4). In general, the stiffer and more deeply exhumed lithologies are overall more erosion-resistant and maintain their channel more readily than younger rocks (Bursztyn et al., 2015).

Ten bedrock channels intersecting the Mohand Range along the northwest Himalayan front were investigated by Allen et al. (2013) to study the lithologic and tectonic controls on bedrock channels (Fig. 5). In the study area, these bedrock rivers travel southwest from a divide through Upper Siwaliks quartzite-cobble conglomerate with a sand matrix, and across older Middle Siwaliks of poorly indurated multistory sandstone before flowing through a transitional contact (Fig. 6) (Kumar and Ghosh, 1991; Kumar, 1993). A type N Schmidt Hammer, which measures the rebound values (Cargill and Shakoor, 1990; Selby, 1993), and the simple means

test, which is used for substitution of a Schmidt Hammer when measuring weak lithologies (Goudie, 2006), were employed to estimate rock strength in these ten bedrock rivers (Allen et al., 2013). Allen et al. (2013) found that Middle Siwaliks overall has a high rebound value indicating a stronger rock strength and is less erodible than Upper Siwaliks. As a result, the downstream Middle Siwaliks channels are narrower and more steepened than the upstream Upper Siwaliks (Allen et al., 2013). This indicates that rivers narrow their channel width in response to an increase in substrate strength (Allen et al., 2013).

Bedrock river banks and beds are not always submerged underneath water. The water level rises or falls depending on the rate of precipitation, runoff, and evaporation year-round. This forces bedrock channels to undergo episodic wetting and drying in which banks and parts of the bed may be immersed under water in high flows but exposed subaerially during some or most of the year. The minerals inside the bedrock thus undergo cycles of hydration and dehydration leading to expansion or contraction, which can decrease rock competence and disaggregate the bedrock. This common physical process is called slaking and it can quickly turn indurated, erosion-resistant clastic sedimentary rocks into sediment in just a year to decades, imposing a strong impact on the lithologic strength of bedrock meandering rivers.

Montgomery (2004) summarized the impact of slaking on bedrock channel erosion. He recognized that slaking causes asymmetry between sub-aerial bedrock and submerged bedrock in bedrock erodibility. When weak sedimentary bedrock is susceptible to cyclic wetting and drying, bedrock submerged under water maintains the rock strength while bedrock exposed becomes weaker (Montgomery, 2004). Erosion rates in the subaerial zone can be 10 times higher than in the subaqueous (Collins et al., 2016). Water will quickly erode the exposed rock until the bedrock reaches low-flow water level and becomes continuously submerged; this process rapidly

lowers the bedrock channel, increases lateral erodibility, and widens valleys (Montgomery, 2004; Collins et al., 2016).

The wetting and drying cycles were further quantified by Inoue et al. (2017) who collected fresh bedrock samples at nine locations along eight rivers in Hokkaido, Japan, and artificial weathered them to simulate the changes in tensile strength that occur during wet-dry cycles. The increased number of wet-dry cycles results in a weaker tensile strength (Fig. 7) although the reduction in tensile strength depends significantly on the bedrock type (Inoue et al., 2017). Sandstone samples from the Sorachi River (So) decreased in tensile strength slightly after repeating 10 wet-dry cycles (Fig. 8). In contrast, sandstone from Saranbe River (Sr) showed a dramatic decrease in tensile strength after only two wet-dry cycles (Fig. 8).

Here, I study the effect of lithologic-dependent erosion styles—namely, the contrast in vertical and lateral rock strength—on the stability of bedrock meandering channels. Results from this work will determine the lithologic characteristics that support meandering bedrock channels as opposed to braided channels, thus informing where planform-specific ecologic niches may develop. Overall, my research will allow other researchers to understand how topographic evolution responds to lithology and it will aid our broader understanding of global topographic change.

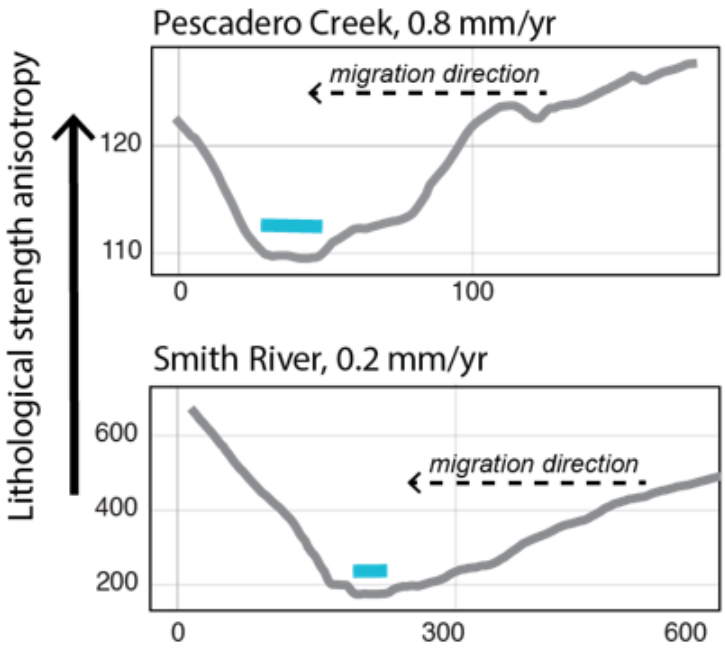

Figure 3. Valley morphology in two meandering bedrock channels reflects lithologic strength characteristics: the two rivers pictured above illustrate how meander cross-sections can vary based on lithology and uplift rates (Schanz and Yanites, 2020 NSF Proposal).

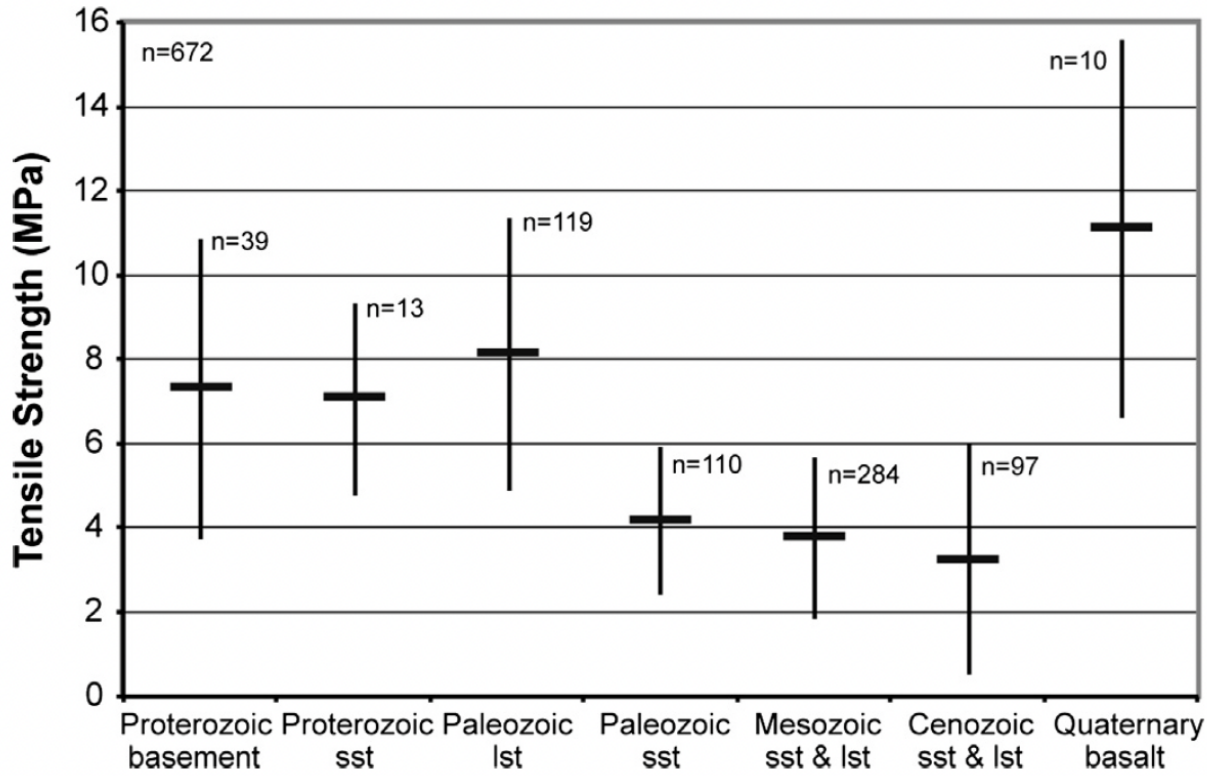

Figure 4. Means and standard deviations of tensile rock strength show a decrease of geologic age and burial depth from left to right, except for indurated younger basalt and limestone (Bursztyn et al., 2015).

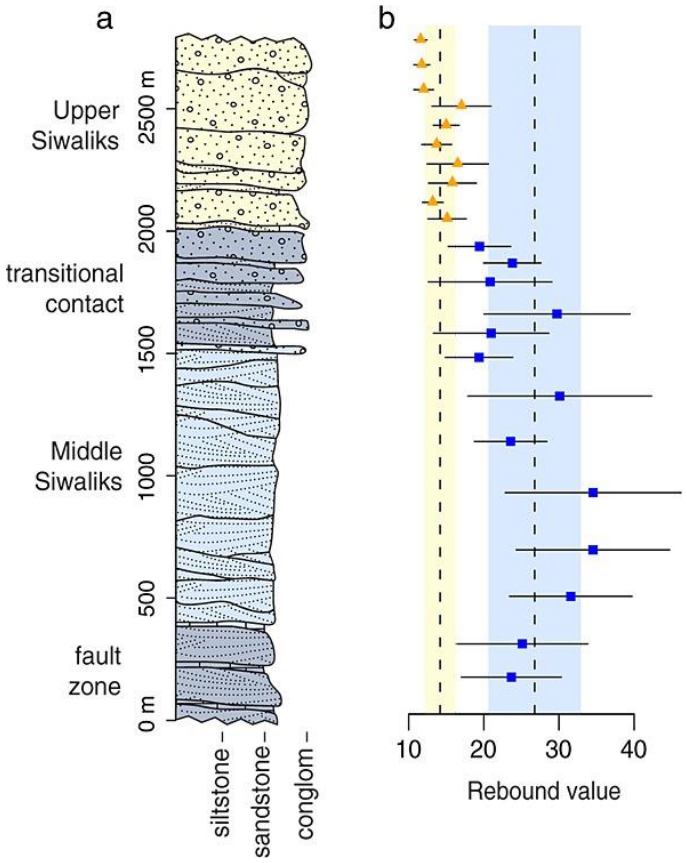

Figure 5. (a) Central Mohand stratigraphic column (Allen et al., 2013; modified from Kumar [1993]) (b) Rebound values measured from Schmidt Hammer in the Upper Siwaliks and the middle Siwaliks. Dashed lines are lower means (Allen et al., 2013).

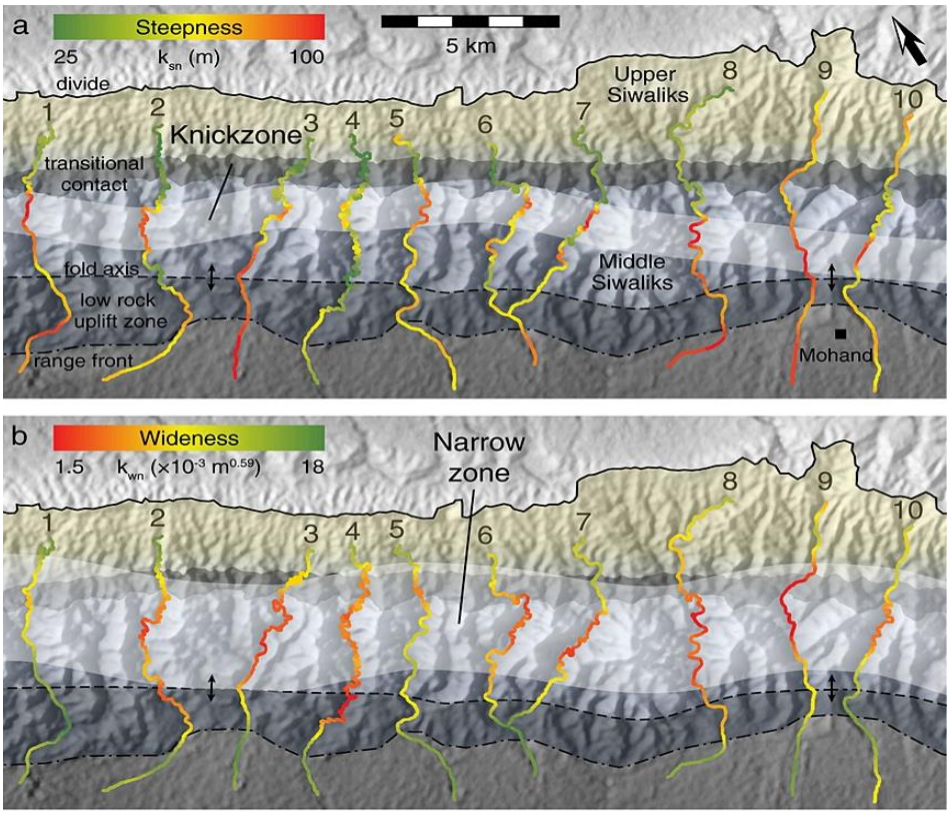

Figure 6. Planview patterns of smoothed channels that show the distribution of normalized steepness index (*ksn*) (a) and normalized wideness index (*kwn*) (b) in each channel (Allen et al., 2013).

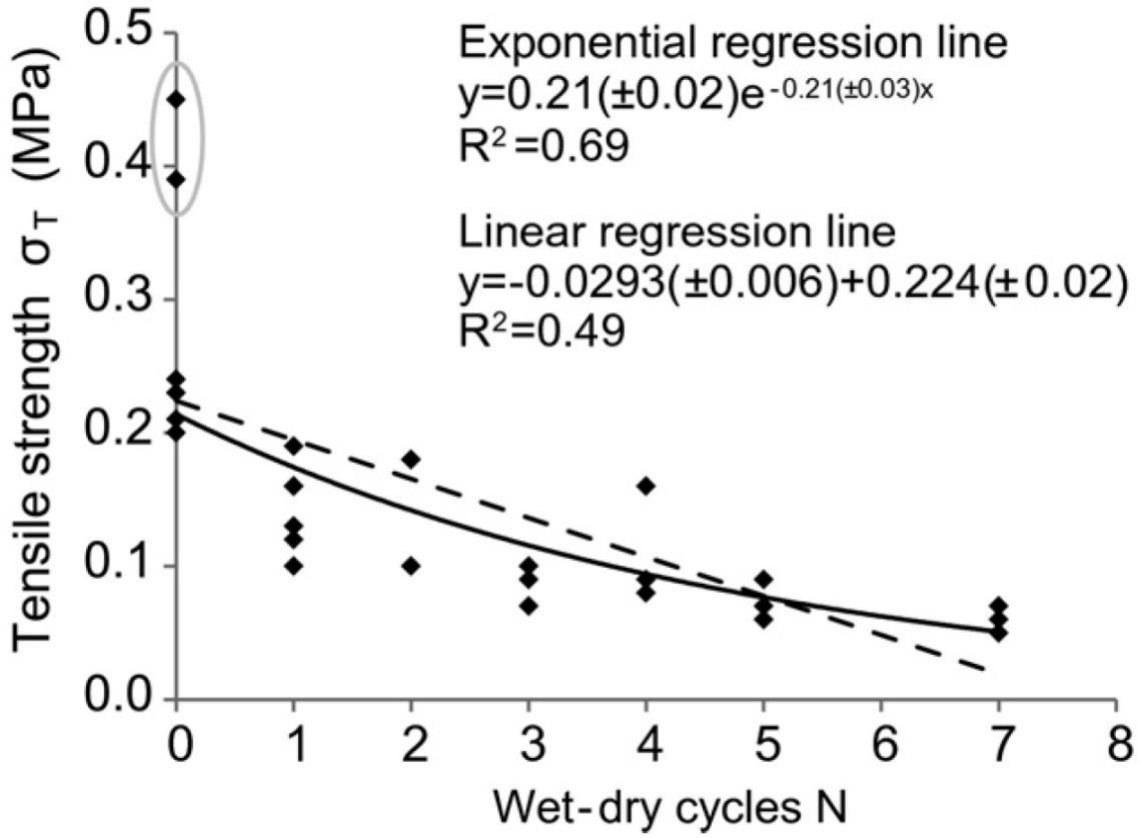

Figure 7. The sampled rocks decrease their tensile strength while experiencing more wet–dry cycles (Inoue et al., 2017). The dashed represents a power regression line, whereas the black line represents a linear regression (Inoue et al., 2017).

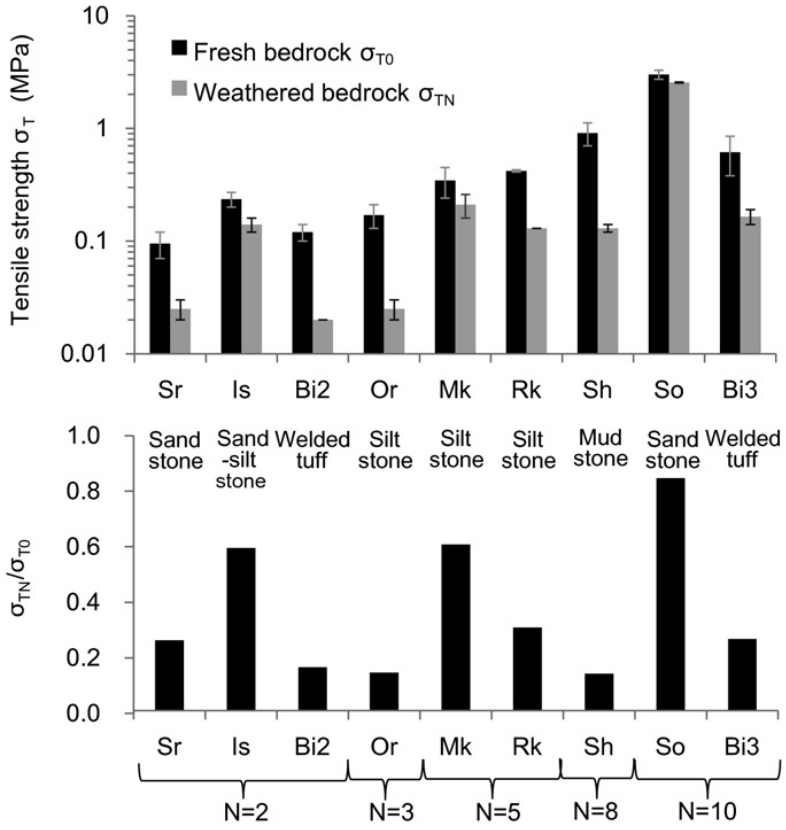

Figure 8. Variations in tensile strength due to recurring wet–dry [n-dash, not hyphen] cycles, where *σT0* is median tensile strength of initial (fresh rock), σTN is tensile strength of artificially weathered bedrock, and N indicates the number of wet–dry cycles (Inoue et al., 2017). The x-axis denotes rock samples collected from different rivers. The names of the rivers are abbreviated.

STUDY AREA BACKGROUND

Smith River

The simulated river channels do not replicate reality, but rather show the relationship between input variables such as climate and lithology, and output variables such as erosion rates and channel sinuosity. However, using a real river as a basis for the input provides a physical constraint to the model, and allows one to compare simulated channel evolution with actual trends. The Smith River in Oregon (Fig. 9) has been chosen as a study site due to its active meanders, unpaired clear meander loop terraces that preserve meander features (Finnegan and Dietrich, 2011, Personius et al., 1993), and low bedload production rate (O'Connor et al., 2014), all of which suggest that the river was historically a bedrock river and is expected to remain single-threaded. This site is an ideal location for study because it displays evidence of long-term bedrock meandering (Schanz and Yanites, 2020 NSF Proposal). It is also believed to be in topographic steady state (Kelsey et al., 1994, Reneau and Dietrich, 1991)—simplifying model assumptions about sediment supply and erosion—and is unlikely to be impacted by recent anthropogenic activity that may influence bedrock erosion processes (Schanz and Yanites, 2020 NSF Proposal).

Physical Features

The Smith River is one of the largest tributaries of the Umpqua River in Oregon State, USA. It drains 900 km^2 (SRWA, 1997), and is approximately 140 km (90 miles) long, entering the Umpqua River about 18.5 river kilometers (RK) (11.5 river miles (RM)) from the coast, near

Reedsport, OR. It is situated on the Pacific Ring of Fire and located within the Central Oregon Coast Range. The river originates in the Calapooya Mountains at an elevation of approximately 1,219 meters (4000 feet) and flows for approximately 121.5 kilometers before joining the Umpqua River; within our study area, total relief is approximately 396 meters (1300 feet).

Geology

The Smith River flows through Coast Range Sedimentary Rocks, which are mainly composed of arkosic sandstone and siltstone of the Eocene Tyee Formation and scattered mafic volcanic and intrusive Eocene and Oligocene rocks (Walker and Duncan, 1989; Walker and MacLeod, 1991). The lithology along this river channel is very uniform, e.g., few lithologic complexities. Multiple analyses, such as clast attrition experiments and bed material yield analyses, indicate that the Smith River bedrock substrate is softer compared with other geologic provinces further to the east (O'Connor et al., 2014) (Fig. 9).

The uplift of the Oregon Coast Range (OCR) began during the Miocene due to the reorganization of the Pacific and Juan de Fuca Plate (McNeil et al., 2000). This has resulted in ongoing subduction that drives rock uplift in the OCR, with the Cascadia Subduction Zone now located 60–100 km west of the Coast Range (Kobor and Roering, 2004). Due to the proximity to the Cascadia subduction zone, the topography of Oregon has been constantly changing, and it experienced episodic eustatic changes and long-term uplift throughout the last 100,000 years (Carver et al., 1985; Kelsey, 1990; McInelly and Kelsey, 1990). Based on recent geodetic data from the last 40–70 years, uplift rates in the central and northern Coast Range typically range from 0 to 4 mm per year (Mitchell et al., 1994; Personius, 1993). Geodetic rates decrease in a north–northeast direction from 3 mm/year south of Reedsport to 1 mm/year north of Florence

(Mitchell et al., 1994; Personius, 1993). In contrast to the short-term uplift rate, marine terraces along the Oregon coast record uplift over the last 80 – 125 kyr with a low uplift rate of less than 0.4 mm/year (West and McCrumb, 1988; Kelsey, 1990; McInelly and Kelsey, 1990; Muhs et al., 1990; Ticknor, 1992; Kelsey and Bockheim, 1994; Kelsey et al., 1994; Personius, 1993), except in areas where late Quaternary faults displace marine wave-cut terraces(West and McCrumb, 1988). Variations in uplift over millions of years may be reflected in the broad regional differences in topography (Kelsey et al., 1994). However, my study area is positioned where it shows little to no systematic variation in long-term rock uplift rate.

The Geologic Map of Oregon includes a few unpaired Quaternary surficial deposits that are composed of mixed grained sediment at the outside bank of the river channel (Baldwin, 1956). The rocks found along the Smith River channel formed by a sequence of turbidity currents in the deep sea and subsequently brought to the surface above sea level (Niem and Niem, 1990). The map shows no signs of major landslides; however, due to the slope form and gradient, the area is susceptible to landslides (SRWA, 1997). There is no evidence of a fault, but several N–S-trending folds have been discovered near the Smith River channel, which flows in an E–W direction.

Climate

The Smith River watershed area is characterized by cool and wet winters, whereas summers are relatively dry (SRWA, 1997). According to data obtained from the USGS (StreamStats – USGS Web Application for Basin and Streamflow Characteristics, n.d.), the mean annual minimum air temperature was 5.7 °C (42.2 °F) in 2008, while the mean annual maximum air temperature was 16.9 °C (62.5 °F) during the period from 1971 to 2000. The mean annual

precipitation (MAP) is 1460.5 mm (57.5 inch). Since there is no mean annual air temperature (MAAT) being reported from Streamstats in our study area, the MAATs of two cities, Reedsport and Elkton, which are in proximity to the study area, are employed based on the climate data provided by Climate-Data.org using European Centre for Medium-Range Weather Forecast (ECMWFF) model. From 1991 to 2021, Reedsport averages 11.5 °C (52.6 °F) and Elkton averages 10.9 °C (51.7 °F). The MAP of Reedsport and Elkton is 1393 mm (54.8 inch) and 1397 mm (55.0 inch), respectively, with most of the precipitation occurring from October to April (Climate-Data.org) and only a small percentage in summer.

The Smith River is in the Klamath–Siskiyou ecoregion. This region is known for its high biodiversity, including numerous endemic plant and animal species. The riparian community along the Smith River is characterized by the dominance of red alder (*Alnus rubra*) trees, which provide a canopy for an understory of sword fern (*Polystichum munitum*), salal (*Gaultheria shallwon*), and vine maple (*Acer circinatum*) (Gunckel et al., 2006). Several fish taxa are present in our study area, including Pacific and western brook lampreys, coho salmon (*Oncorhynchus kisutch*), Chinook salmon (*Oncorhynchus tshawytscha*), steelhead, coastal cutthroat trout (*Oncorhynchus clarkii*), large-scale sucker (*Catostomus macrocheilus*), redside shiner (*Richardsonius balteatus*), longnose dace (*Rhinichthys cataractae*), and Umpqua pikeminnow (*Ptychocheilus umpquae*) (Gunckel et al., 2006).

Land-Use History

According to O'Connor et al. (2014), the typical land-use perturbations in the Pacific Northwest, such as dams, timber harvest, fire, in-stream and floodplain gravel mining, placer mining, and local channel and floodplain development, have affected aspects of the Smith River

to some extent. The land-use map from ArcGIS Living Atlas of the World shows that between 2017 and 2022, the Smith River area has experienced a significant conversion of forest land to bare land, primarily due to timber harvesting. Hance et al. (2016) reported that human activities along the West Fork Smith River, such as splash damming until 1935, have led to a reduction in instream wood and bedload. However, Miller (2010) found no evidence of splash dams on the mainstem Smith River or upstream of the study area, indicating that the direct modification of the channel was not intense in our study location.

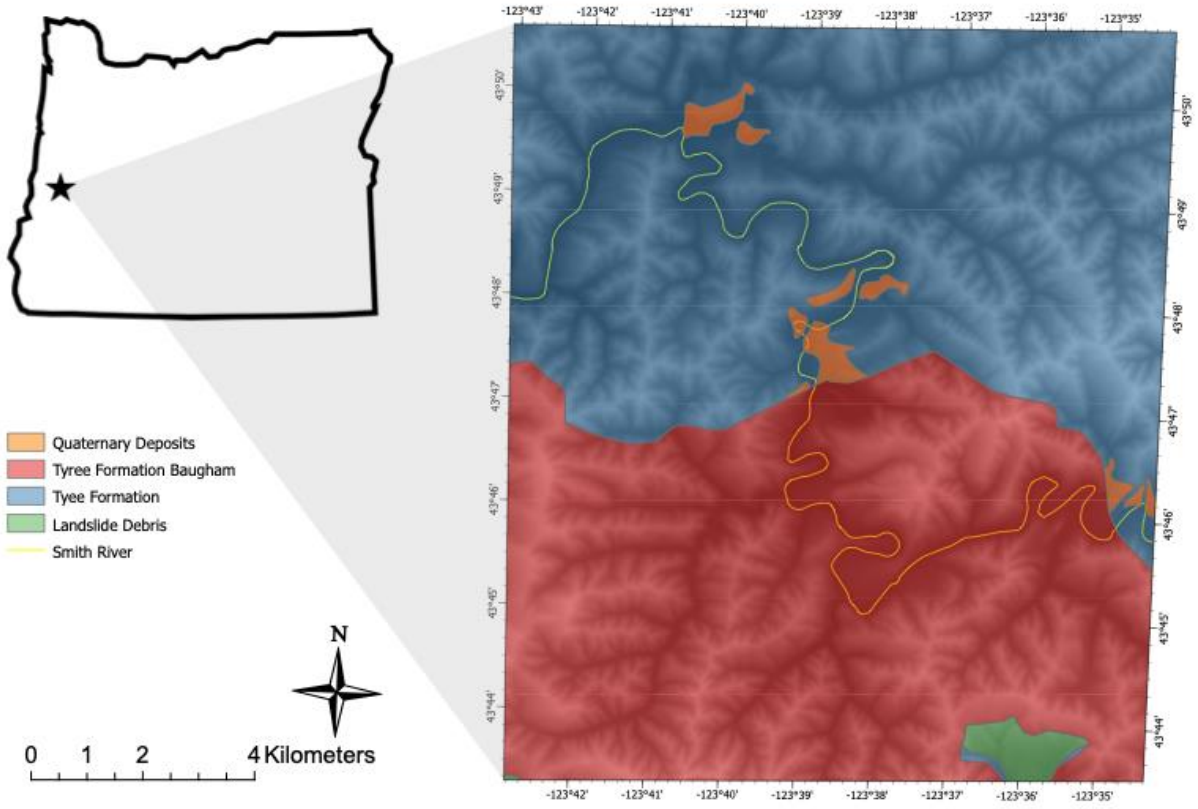

Figure 9. Geologic map of the study area, which is a north–south trending reach of the Smith River. The map shows the distribution of geological features and formations in the study area.

METHODS

In order to understand the role of lithology in facilitating migration and maintaining the stability of meandering bedrock rivers, I apply a numerical model that was developed by Drs. Sarah Schanz and Brian Yanites. This model is a 1-D numerical model but also incorporates some 2-D variables, such as channel width and channel x–y position. The model was originally designed to test the predicted relationship between channel threads and rock uplift rates, bedrock strength anisotropy, and sediment supply/transport capacity. For my project, which specifically focuses on bedrock type and strength, the effects of variables *kl* (lateral erodibility), *kf* (vertical erodibility), *channel type* (channels with different shapes and widths), and initial slope (the initial slope of a channel) on the rate and sinuosity of simulated meanders are analyzed, while holding the other variables contained in this model constant. This allows for testing of sensitivity of bedrock meandering development to lithologic strength differences (kl, kf) and lithologic controlled slopes (*initial_slope*).

Lateral Erodibility and Vertical Erodibility (*kl & kf*)

In this model, *kl* and *kf* are empirically derived lateral and vertical erodibility, respectively. The product of lateral erodibility *kl*, channel width, and channel curvature is the lateral erosion rate, and the product of vertical erodibility *kf* and shear stress modulated by sediment transport capacity is the vertical bedrock incision rate.

Lateral erosion rates in bedrock channels are not well-studied and have proven challenging to apply on a mechanistic model, and in addition, little to no data on *kl* values exist in published literature (Hancock and Anderson, 2002; Montgomery, 2004). To run this model, *kl* values derived during Colorado College student Parker Rehmus' senior research are employed.

The required parameters for calculating *kl* are uplift rates, slip-off slope, upstream gradient, bank-full discharge and a table of evenly spaced nodes with x-y coordinates and channel width. Uplift rates were obtained from Ivan Beck (unpublished research, 2022). Slip-off slope and upstream gradient are calculated from the digital elevation models in Google Earth. Bankfull discharge is collected from global stream gauge data. Lastly, evenly spaced nodes with x-y coordinates and channel width are extracted from a GIS. Using these data, Rehmus predicted the ratio of lateral to vertical erosion rates, preserved as the slip-off slope. Vertical erosion rate is approximated by uplift rate from Beck (2022); lateral erosion rates are estimated using the Howard and Knutson (1984) meandering model, which includes inputs of slope, discharge, channel width, and channel position. The *kl* variable is altered until the Howard and Knutson (1984) predicted lateral migration matches the lateral migration rate encoded in the slip-off surface. In my simulations, I varied *kl* from 0.1 to 0.001, which matches values of *kl* inferred by the previous method of 0.1 to 0.001 for the Clearwater River, WA (Rehmus, 2022 unpublish research).

Vertical erodibility values used in my model, *kf*, are adopted from Yanites (2018) and varied by one order of magnitude higher and lower, in keeping with typical *kf* values used in numerical modelling. I have changed vertical erodibility values within the range of -0.0001 and -0.000001.

Initial Slope

The other independent variable, *initial slope*, is well-constrained by field data and literature. It is a value that represents the slope of a channel, which is dependent on the underlying bedrock strength and regional uplift rate (Burbank and Anderson, 2011). I made a

comparison of initial slopes ranging from 0.005 to 0.00001, which correspond to the gradient values found in various modern rivers. For instance, the steep valleys and narrow canyons of the upper reaches of the Colorado River, Colorado, USA have a steeper initial slope of approximately 0.005, while the source of the Mississippi River located in northern Minnesota, USA has a gentler initial slope of approximately 0.00001.

Channel Type

There are three types of bedrock channel morphologies were simulated in this model: *trapezoidal*, *rectangular*, and *nochange*. Trapezoidal and rectangular channel type are the end members of channel evolution pattern. For the trapezoidal channel type, the channel cross section integrates lateral and vertical erosion rates to form a trapezoid shape, with bank slopes representative of prior lateral and vertical erosion. For the rectangular channel type, only the channel width will grow with any lateral erosion because there is no mechanism to narrow the channel. Thus, such channels are predicted to turn into braided channels (Finnegan and Balco, 2013). These two channel types are distinct from the no-change channel type from prior models that maintain constant channel width and height (e.g., Howard and Knutson, 1984; Finnegan and Dietrich, 2011); this assumption is valid for alluvial rivers but not necessarily for bedrock rivers.

Expected Model Output

To test the sensitivity of bedrock meandering processes to the aforementioned variables, I ran three sets of the model with different channel types (*no change*, *rectangular*, and *trapezoidal*). Under each channel type, five groups with different lateral and vertical erodibility

values, and one group of the model with variable initial slope values, were run for 100 ka, using the supercomputers from Indiana University. With a total of eighteen groups, each group contains five model runs, resulted in a total of 90 channel simulations.

After the model runs were completed, the generated data files were stored in a pre-designated repository. I wrote Python scripts to analyze the relationship between each independent variable in the model. Each Python script allowed me to analyze a simulated channel from different aspects:

1) The temporal evolution of the channel in planview (Fig. 10) provides a straightforward view of the simulated bedrock meandering river and the river channel history of migration and cutoff development during the model run time.
2) The relationship between sinuosity and model time (Fig. 11). Sinuosity reflects the longitudinal channel morphology. Increasing sinuosity over time indicates that the channel grew more meandering, while decreasing in sinuosity might indicate that the river channel transforms from a meandering river channel to a braided river channel.
3) Lastly, the relationship between values of kl/kf/initial slope and model time (Fig. 12). This shows the temporal evolution of the channel, with particular attention paid to meander cutoffs—as a measure of meander stability—over time.

Numerical Model

The model's framework is to generate a lateral erosion rate and vertical erosion rate, at each time step, in a coordinate system. There are six core functions to run the model. First, vertical erosion is dependent on shear stress τ_b:

$$\tau_b = \rho_w g H S$$

where ρ_w is the density of water, g is gravitational acceleration, H is the flow depth, and S is the slope of channel bed.

The water depth at bankfull discharge is approximated using the wide channel assumption and estimated with Manning's equation:

$$\begin{cases} H = \left(\frac{n * Q_w}{W}\right)^{0.6} (-1 * S)^{-0.3} \text{ if } S < 0 \\ H = 0 \text{ if } S \geq 0 \end{cases}$$

where Q_w is the bankfull discharge, W is the channel width, and n is Manning's roughness.

The basal shear stress, τ_b, (equation 1) is a proxy for bedrock erosion potential, and is commonly employed in bedrock detachment-limited models (Howard & Kerby, 1983; Whipple & Tucker, 1999):

$$E = k_f \tau_b dt$$

where E is the erosion rate, k_f is an empirical constant that includes lithologic properties (Whipple et al., 2000), and dt is the time step.

Channel Migration and Meandering

Meander migration is driven by curvature, following Howard and Knutson (1984). Planview curvature is calculated at each node of the model:

$$c = \left(\frac{dxddy - dyddx}{(dx^2 + dy^2)^{1.5}}\right)$$

where dx and dy are the first derivative of planview x and planview y, respectively; ddx and ddy are the second derivative of planview x and planview y, respectively.

The nominal migration rate, R_0, at each node of the stream is calculated from curvature, channel width, and the lateral erosivity *kl* (Howard and Knutson, 1984):

$$R_0 = Wk_lc$$

The adjusted migration rate, R_1, is calculated by weighing the nominal migration rates, R_0, for the current and upstream locations at the location s, the distance measured from the mouth of the simulated stream (Howard and Knutson, 1984):

$$R_1(s) = \Omega R_0(s) + \left[\Gamma \int_0^\infty R_0(s-\xi)G(\xi)d\xi\right]\left[\int_0^\infty G(\xi)d\xi\right]^{-1}$$

where $R_0(s-\xi)$, at a distance ξ upstream from s, is the nominal migration rate. Ω and Γ are weighting parameters, and $G(\xi)$ is an upstream weighting function (Howard and Knutson, 1984).

The actual migration rate, R_1', is calculated from the adjusted migration rate R_1 (Howard and Knutson, 1984):

$$R_1' = R_1\mu^\varepsilon$$

where μ is sinuosity and ε is a numerical value, $-2/3$, that was determined by Howard and Knutson (1984).

RESULT

For all the numerical runs, each simulated channel planform starts with the exact same shape with a sinuosity of 1.42. Based on different parameters the model received, each simulated channel ended up with a distinct channel geometry at 100,000 model years. The specific variables, including lateral erodibility, vertical erodibility, initial slope, and channel geometry, are held constant individually in the subsequent sections, and the results will be presented accordingly.

The units of the erodibility parameters – lateral erodibility (*kl*), and vertical erodibility (*kf*) –are considered as empirical coefficients, and their units are determined by a model or equation and are not dependent on physical properties. The units of the parameters will be mentioned below, and from this point forward, I will refer to them without including the units throughout the rest of the section. *kl* is expressed in units of meters per year (m/year), which represents lateral erosion potential over a given period. *kf* is expressed in units of $m^2s^2kg^{-1}yr^{-1}$, which represents vertical erosion potential over a given period for a shear-stress bedrock erosion model.

Lateral Erodibility (*kl*)

In order to examine the effect of lateral erodibility on meandering processes, vertical erodibility, *kf*, was maintained at a constant value, the initial slope was established at 0.0001, and the channel type was set to no change.

General Trends

The channel planforms produced with a *kf* value of -0.000001 displayed an increasing sinuosity over time for simulations with the higher *kl* values of 0.1 and 0.05 (Figure 10). In contrast, *kl* values of 0.01, 0.005, and 0.001 resulted in less sinuous channel planforms (Figure 10), although all showed an increase from the original sinuosity of 1.42. These sinuosity groups are evident from the beginning of the simulation, where simulations with *kl* of 0.1 and 0.05 quickly gain sinuosity, while the lower *kl* grouping remains near 1.42 and slowly increases sinuosity in time (Figure 11). All *kl* values result in linear increases in sinuosity with time, although punctuated decreases in sinuosity are evident when channel cutoffs occur. Simulations with *kl* values of 0.1 and 0.05 had final sinuosity values that were 188.7% and 140.1%, respectively, of the initial sinuosity of 1.42 (Figure 11). However, *kl* values of 0.01, 0.005, 0.001 only displayed a 7.0%, 3.5%, and 0.7% growth, respectively, from the original sinuosity of 1.42 (Figure 11).

A decrease in *kl* results in a decline in the amounts of cutoffs broadly speaking (Figure 12). For the simulations with a *kf* value of -0.000001 (Figure 12), with *kl* value of 0.1, the channel experienced nine cutoffs, while with *kl* values of 0.05, 0.01, 0.005, and 0.001, the channel experienced six, two, zero, and zero cutoffs, respectively. This pattern displays a linear decrease in cutoffs with decreasing *kl* values, until a threshold is reached at *kl* of 0.005.

Exceptions

Whereas the trends discussed above for *kf* of -0.000001 generally hold true, as *kf* varies some trends reverse or experience threshold behavior. Sinuosity through time showed similar trends for *kf* of -0.00001 and -0.000005 (Figures 13-15; Figures 16-18). However, channels created with *kf* set to -0.0001 had opposing sinuosity trends, wherein the lower *kl* values of 0.01,

0.001, or 0.005 exhibited a greater sinuosity than channels with *kl* values of 0.1, or 0.05 at 100 ky (Figure 19). These relative sinuosities begin early in the simulation (Figure 20). The sinuosities in simulations with *kl* values of 0.1 and 0.05 decrease exponentially over time, while low *kl* values of 0.01, 0.005, and 0.001 exhibited a slight linear decrease. The sinuosity of the channel with a *kl* value of 0.05 reduced to 77.5% of its original sinuosity. Conversely, the channel with a *kl* value of 0.01, which has the highest linear decreasing trend, experienced only a 12% decline in its sinuosity.

For all *kf* values used, the number of cutoffs during the 100 ky simulation decreases with decreasing *kl* values, as discussed for a *kf* of -0.000001. However, while the cutoff-*kl* relationship was linear for *kf* of -0.000001, most *kf* values showed a non-linear decrease (Figures 15, 18, 21, 24). In general, a decrease in *kl* value produced less cutoffs, but under certain conditions, the number of cutoffs stayed the same. This occured most commonly between *kl* values of 0.1 and 0.05, and 0.01 and 0.005.

These exceptions to the general trends tend to occur only at the highest *kf* value of -0.0001 and appear to reflect a threshold condition. The channels with the second highest *kf* values of -0.00005 stayed mostly consistent with the previous mentioned general trends in planform, sinuosity, and cutoffs. The only exception observed for this *kf* value was for a *kl* value of 0.001 (the smallest kl value in the dataset); the general trend was an increase in sinuosity, but for *kf* = -0.00001, there was a trivial decrease of 0.14% from 1.424 to 1.422 (Figure 23).

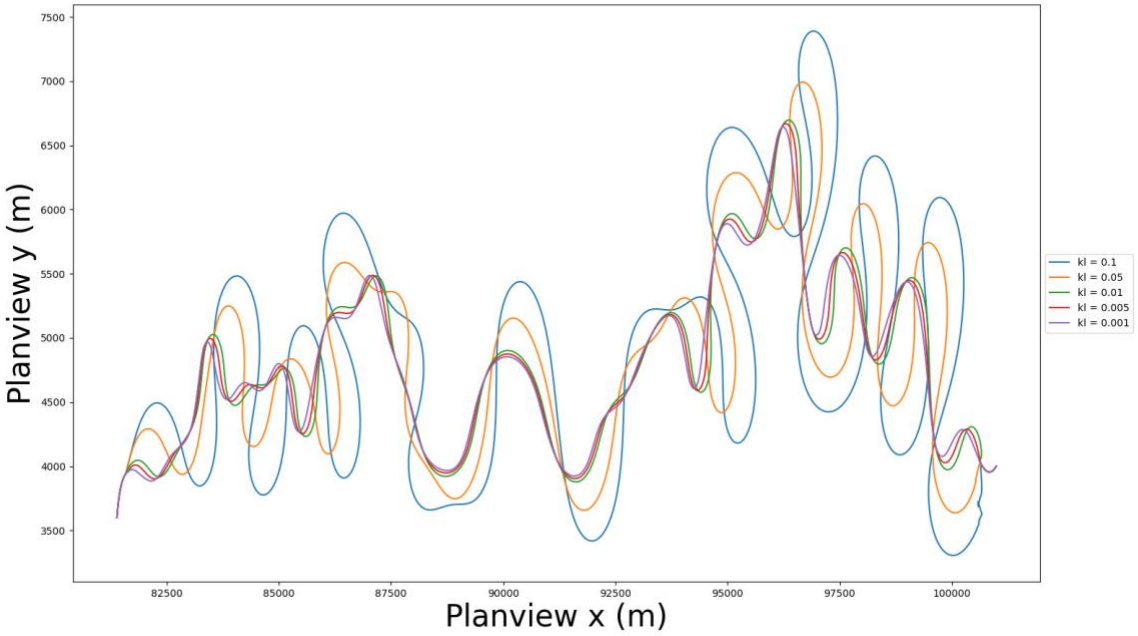

Figure 10. Comparison of planforms at 100 ky for different kl values. kf held constant at -0.000001 while keeping initial slope constant at 0.0001. *No change* channel type has been kept for consistency.

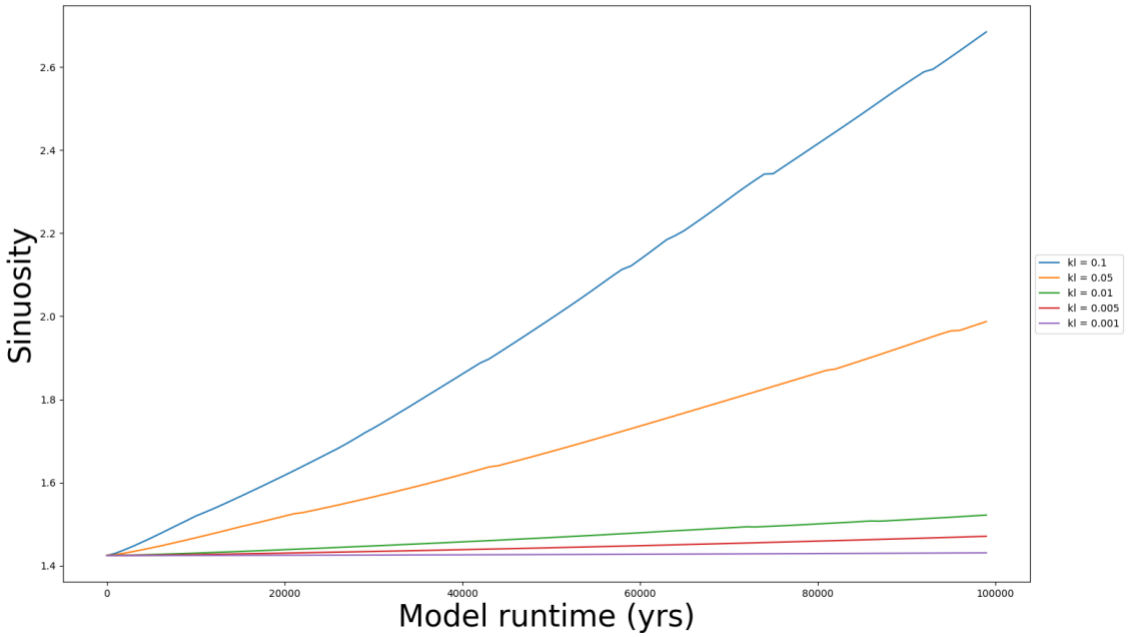

Figure 11. Comparison of sinuosity changes over 100 ky for different *kl* values. *kf* held constant at -0.000001 while keeping initial slope constant at 0.0001. *No change* channel type has been kept for consistency.

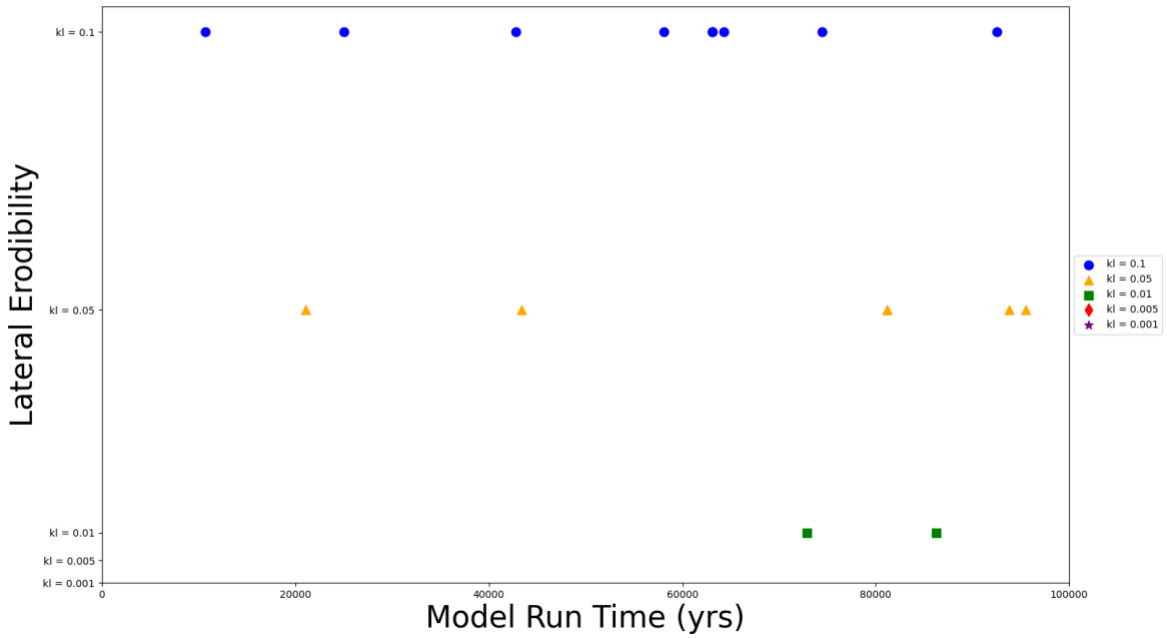

Figure 12. Comparison of cutoff timing over 100 ky for different *kl* values. *kf* held constant at -0.000001 while keeping initial slope constant at 0.0001. *No change* channel type has been kept for consistency.

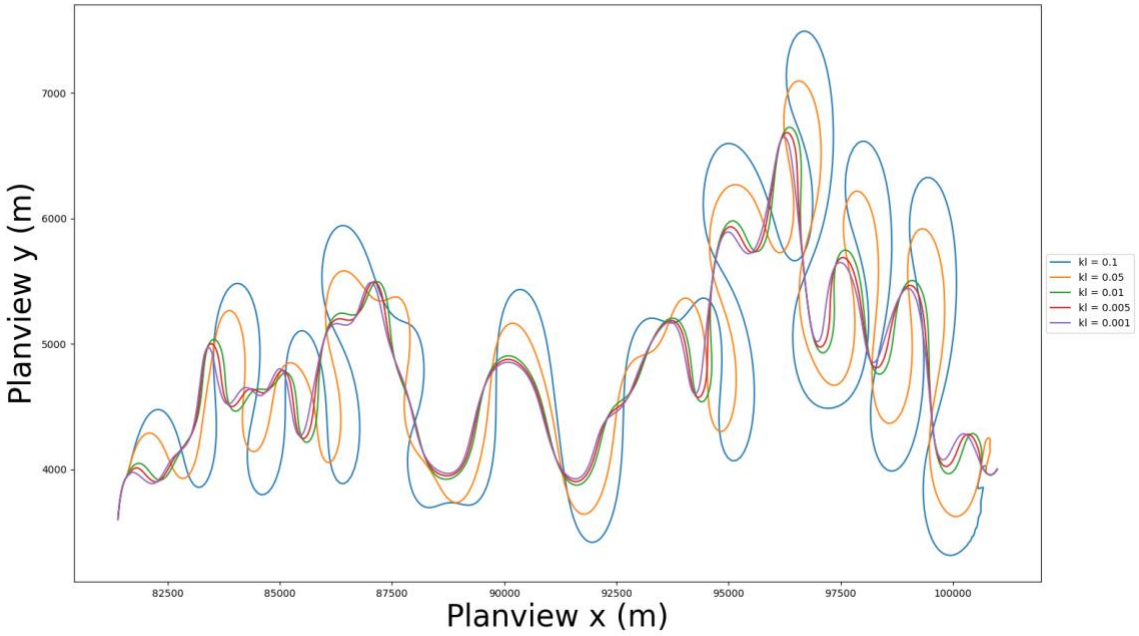

Figure 13. Comparison of planforms at 100 ky for different *kl* values. *kf* held constant at -0.00001 while keeping initial slope constant at 0.0001. *No change* channel type has been kept for consistency.

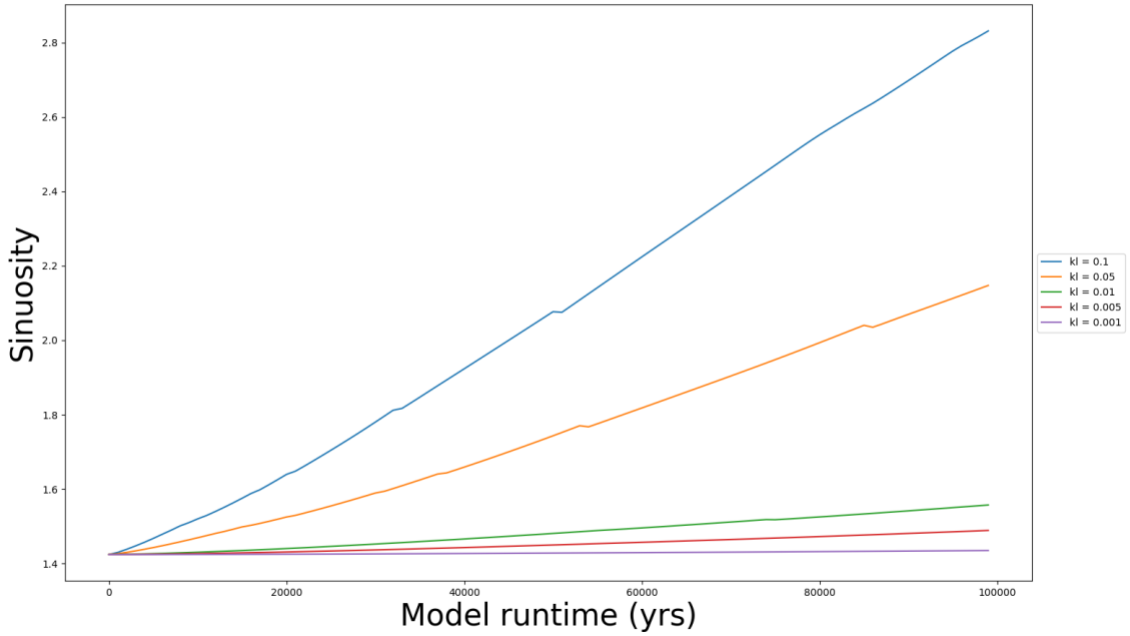

Figure 14. Comparison of sinuosity changes over 100 ky for different *kl* values. *kf* held constant at -0.00001 while keeping initial slope constant at 0.0001. *No change* channel type has been kept for consistency.

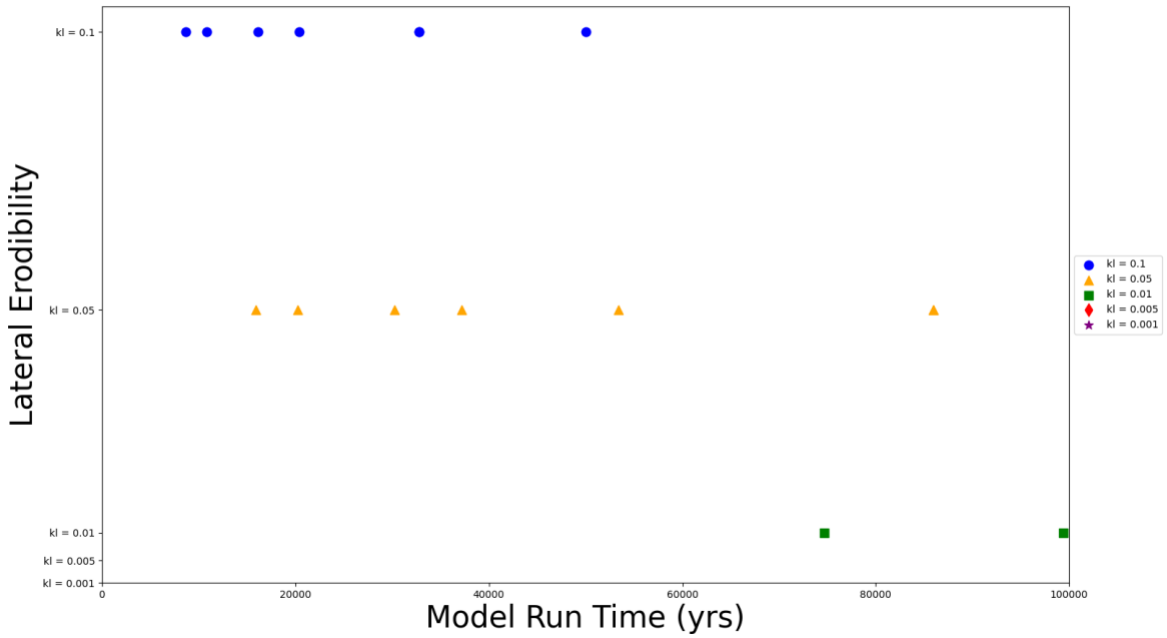

Figure 15. Comparison of cutoff timing over 100 ky for different *kl* values. *kf* held constant at -0.00001 while keeping initial slope constant at 0.0001. *No change* channel type has been kept for consistency.

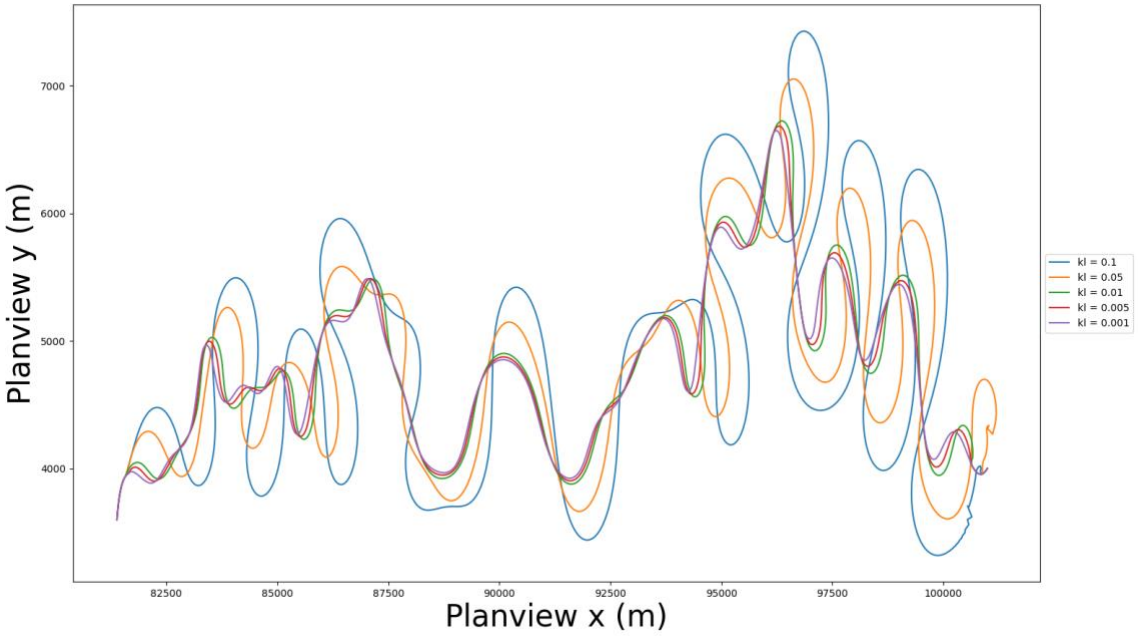

Figure 16. Comparison of planforms at 100 ky for different *kl* values. *kf* held constant at -0.000005 while keeping initial slope constant at 0.0001. *No change* channel type has been kept for consistency.

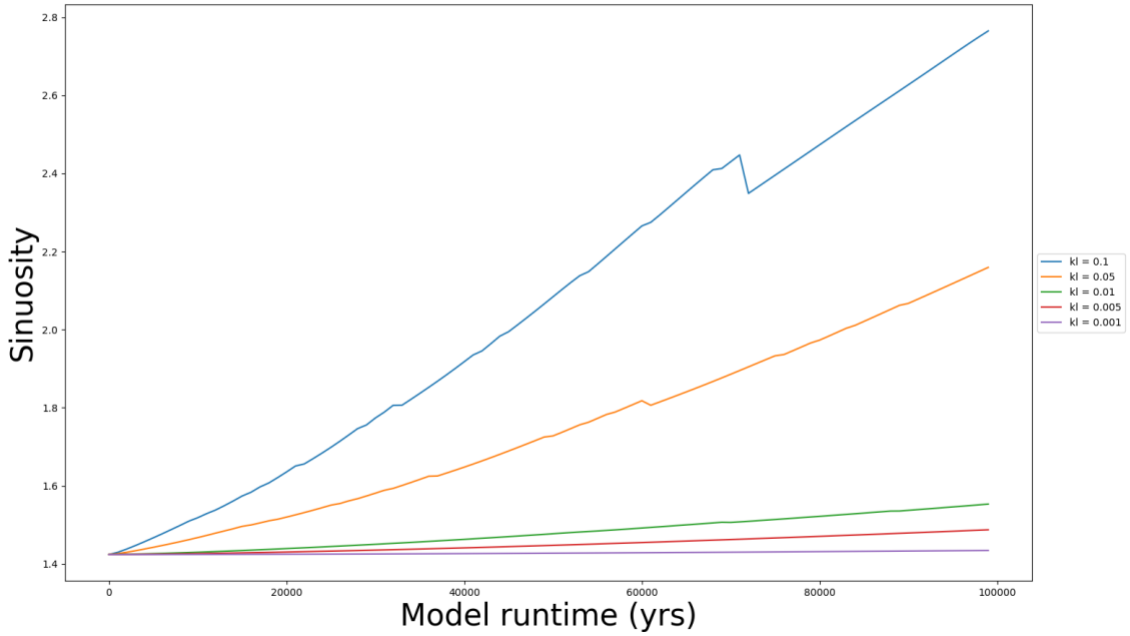

Figure 17. Comparison of sinuosity changes over 100 ky for different *kl* values. *kf* held constant at -0.000005 while keeping initial slope constant at 0.0001. *No change* channel type has been kept for consistency.

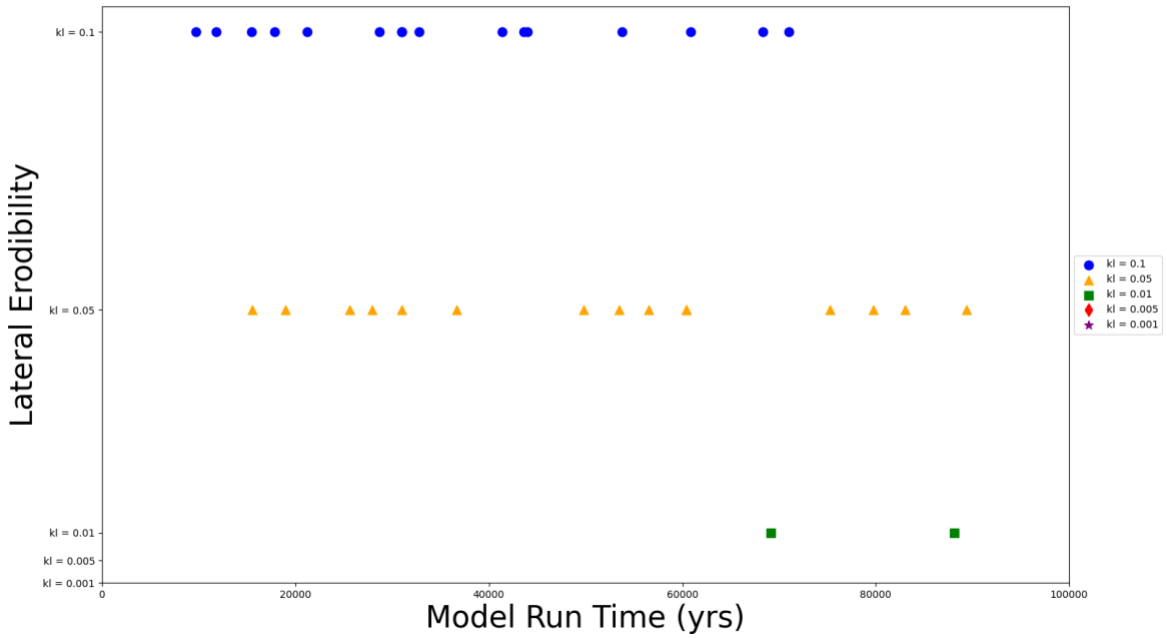

Figure 18. Comparison of cutoff timing over 100 ky for different *kl* values. *kf* held constant at -0.000005 while keeping initial slope constant at 0.0001. *No change* channel type has been kept for consistency.

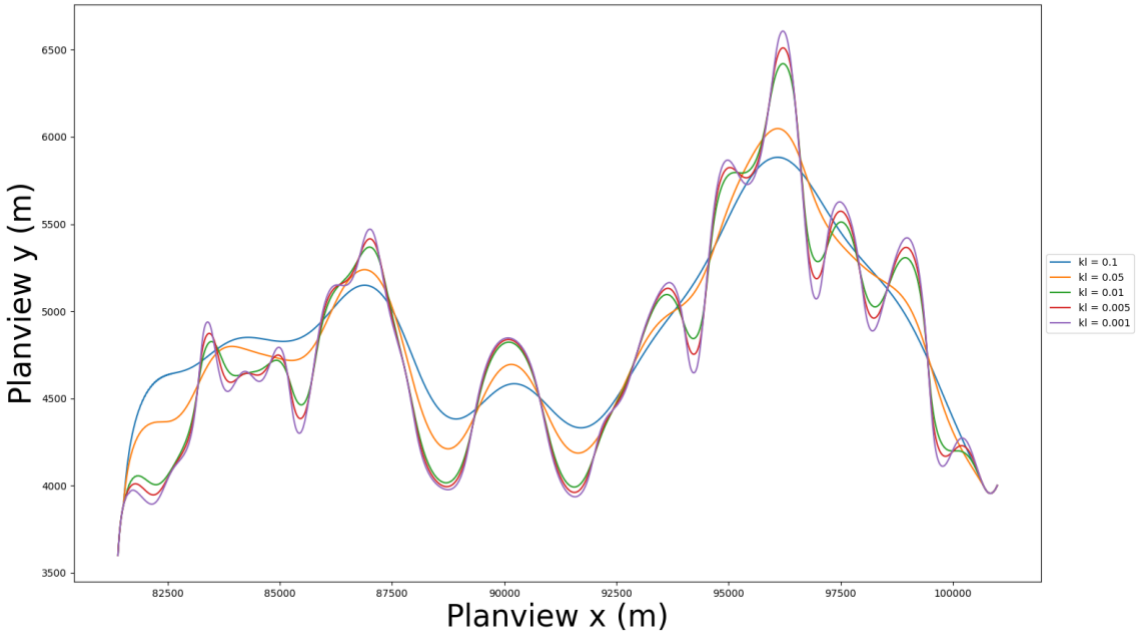

Figure 19. Comparison of planforms at 100 ky for different *kl* values. *kf* held constant at -0.0001 while keeping initial slope constant at 0.0001. *No change* channel type has been kept for consistency.

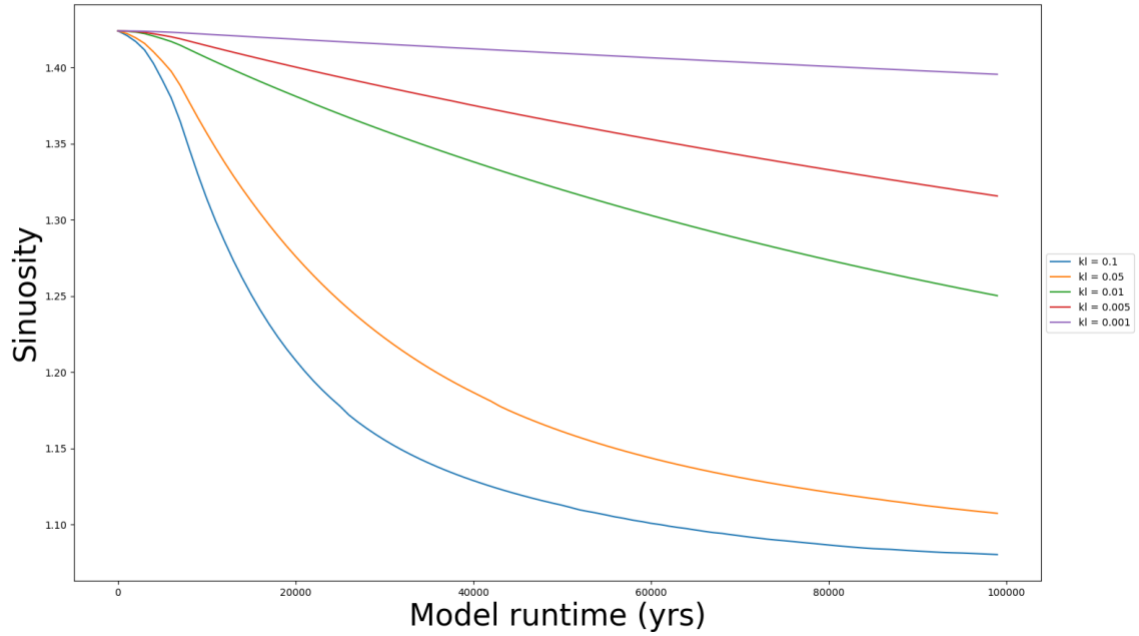

Figure 20. Comparison of sinuosity changes over 100 ky for different *kl* values. *kf* held constant at -0.0001 while keeping initial slope constant at 0.0001. *No change* channel type has been kept for consistency.

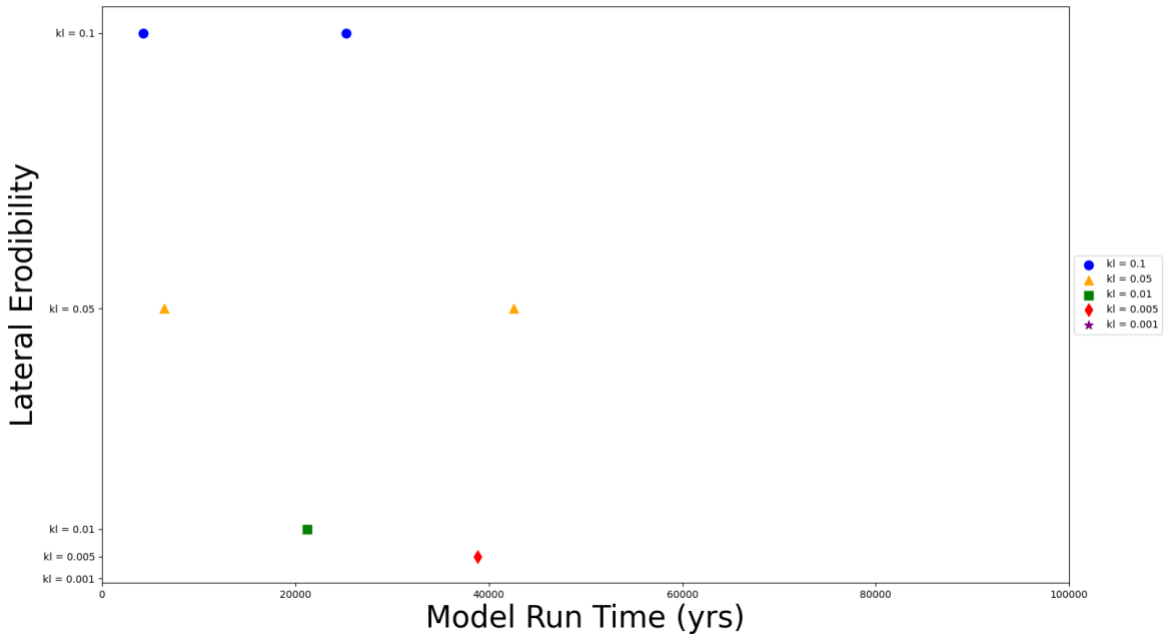

Figure 21. Comparison of cutoff timing over 100 ky for different *kl* values. *kf* held constant at -0.0001 while keeping initial slope constant at 0.0001. *No change* channel type has been kept for consistency.

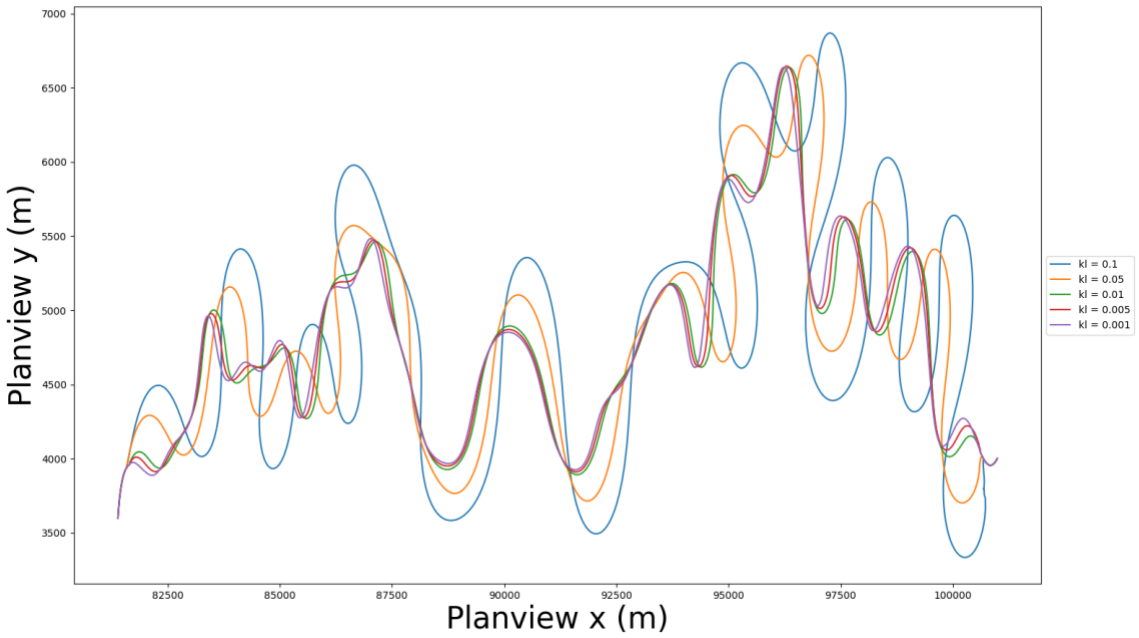

Figure 22. Comparison of planforms at 100 ky for different *kl* values. *kf* held constant at -0.00005 while keeping initial slope constant at 0.0001. *No change* channel type has been kept for consistency.

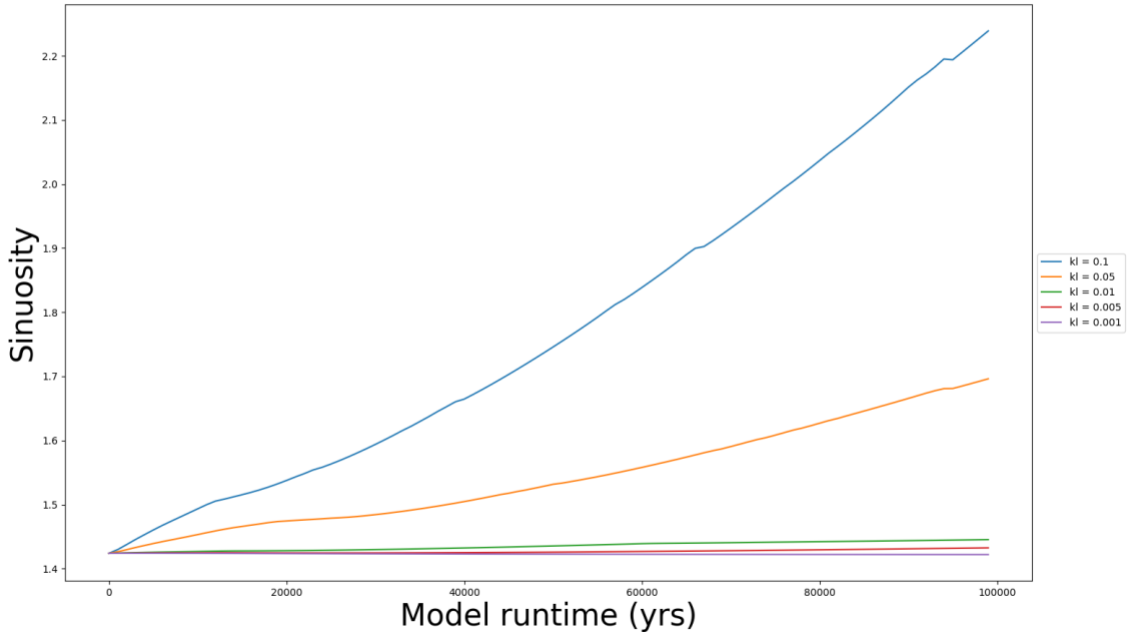

Figure 23. Comparison of sinuosity changes over 100 ky for different *kl* values. *kf* held constant at -0.00005 while keeping initial slope constant at 0.0001. *No change* channel type has been kept for consistency.

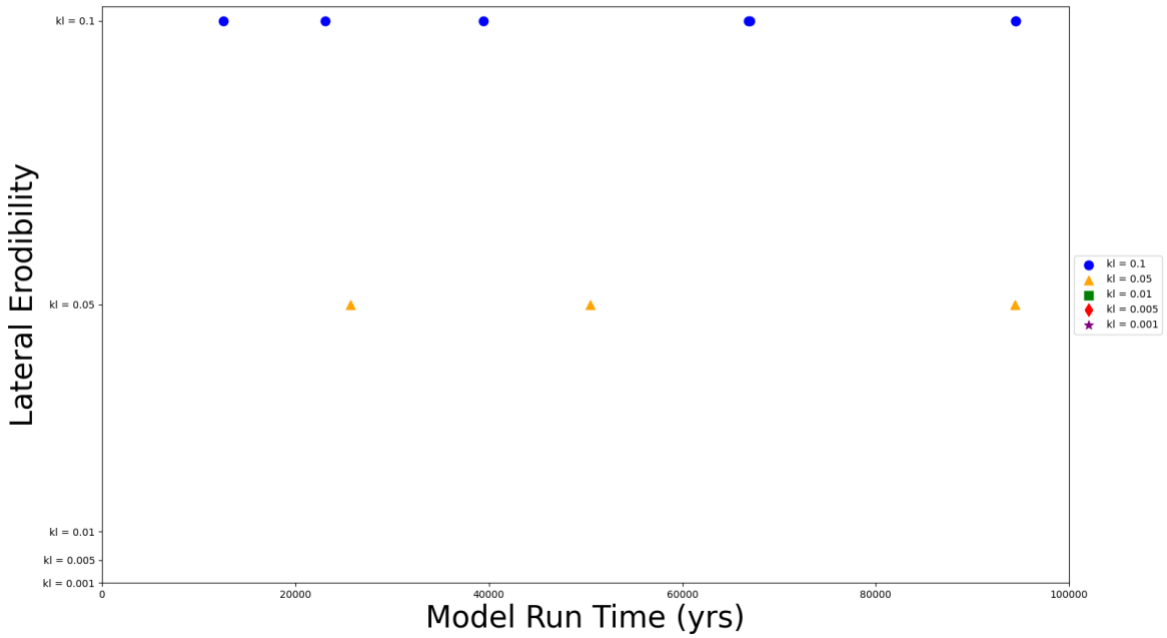

Figure 24. Comparison of cutoff timing over 100 ky for different *kl* values. *kf* held constant at -0.00005 while keeping initial slope constant at 0.0001. *No change* channel type has been kept for consistency.

Vertical Erodibility (*kf*)

General Trends

When the *kl* value was set to 0.01, the number of meanders observed varied depending on the *kf* value used. Specifically, a *kf* value of -0.0001 produced 19 meanders, while the other *kf* values (-0.00005, -0.00001, -0.000005, -0.000001) individually produced 22 meanders (Figure 25). Moreover, the meanders produced by a *kf* value of -0.0001 appeared to be less sinuous than those produced by the other *kf* values. Among the other four *kf* values, there was tight overlap in

the planform for lower *kf* values, while the channel produced by a *kf* value of -0.00005 tended to be less sinuous compared to the meanders produced by the other three *kf* values.

The relative sinuosities can be more directly understood by tracking sinuosity time (Figure 26). The three lower *kf* values immediately grouped together with similar sinuosity values and rates of growth, while the two higher *kf* values displayed their own trends. For *kf* = -0.0001, the simulated channel showed a linearly decreasing trend over 100 ky and it reduced its sinuosity to 1.25, losing 12.0% of the original sinuosity (Figure 26). Some of this sinuosity loss was accounted for in an early cutoff at 20 ky that was only experienced by kf = -0.0001 simulations (Figure 27). The early cutoff for *kf* = -0.0001 led to decreasing sinuosity and a straighter planform by 100 ky. The remaining four kf values, -0.00005, -0.00001, -0.000005, and -0.000001, all depicted a linearly increasing trend (Figure 26). For the *kf* value of -0.00005, the sinuosity changed slightly with an only a 1.4% increase from the initial. *kf* values of -0.00001, -0.000005, and -0.000001 showed increased sinuosity by 9.9%, 9.2% and 7.0%, respectively (Figure 26). While high *kf* values resulted in a lower sinuosity, the highest final sinuosity was at a medium *kf* value, showing the trend between kf and sinuosity is not monotonic and may display threshold behavior. This is consistent with my results with lateral erodibility.

A similar lack of monotonic trends is shown by the cutoffs over time (Figure 27). Whereas the highest *kf* value run experienced one cutoff, the second highest run experienced none, and the three lowest *kf* values all underwent two cutoffs at approximately 70 ky and 100 ky (Figure 27). However, timing of cutoffs appeared random and not correlated to the *kf* value.

Exceptions

The patterns above hold true for most *kl* values, but here I discuss instances where the patterns were reversed. For the lowest *kl* value of 0.001, all planforms are similar (Figure 28).

The sinuosity values for all *kf* values are nearly unvarying, with the greatest sinuosity alteration being a decrease of 2.1% for *kf* value of -0.0001 (Figure 29). When a value of -0.00005 was assigned to *kf*, the planform showed a minor decreasing trend, which is opposite to the increasing trend for the same vertical erodibility in all other simulations. The *kl* = 0.001 planforms did not undergo any channel cutoffs over the course of 100 ky. This suggests that very low lateral erodibility results in a fairly stable channel, regardless of the vertical erodibility value.

As the *kl* value increased to 0.005, the general trends remained the same and stable channels continued; all *kf* values experienced no channel cutoff, except for a run with a *kf* value of -0.0001, which experienced one cutoff (Figure 30).

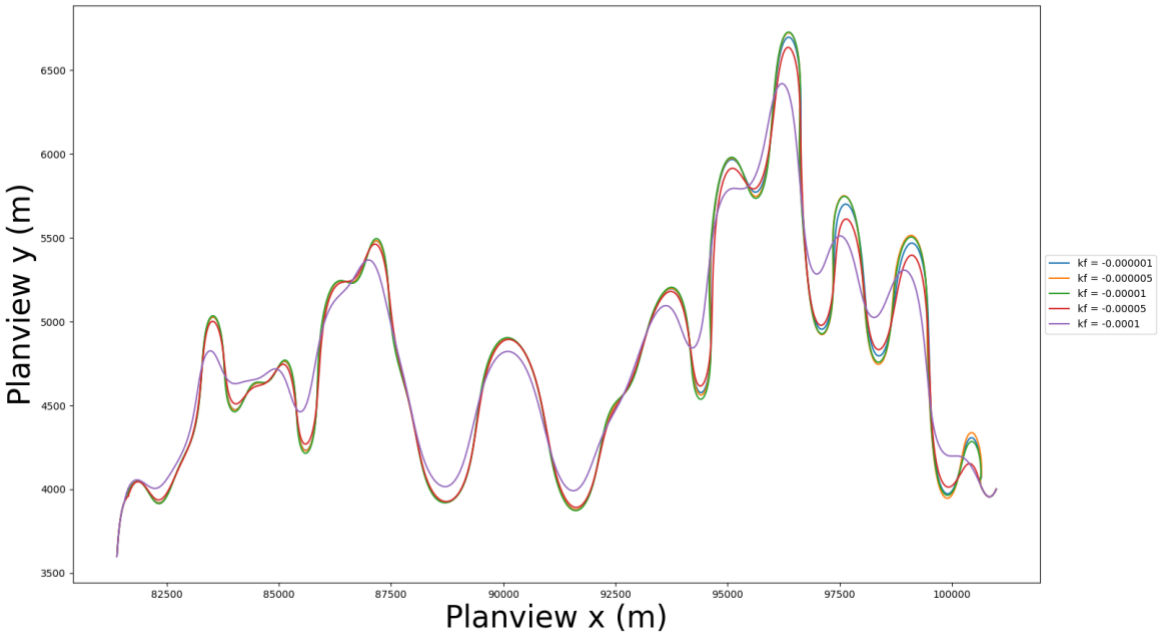

Figure 25. Comparison of planforms at 100 ky for different *kf* values. *kl* held constant at 0.01 while keeping initial slope constant at 0.0001. *No change* channel type has been kept for consistency.

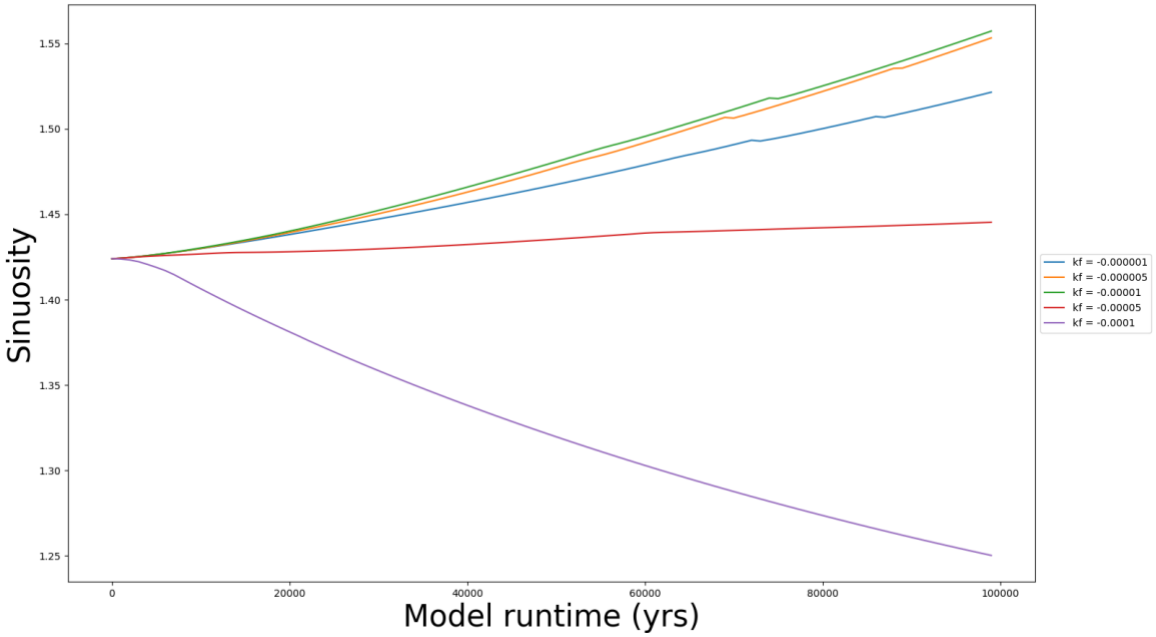

Figure 26. Comparison of sinuosity changes over 100 ky for different *kf* values. *kl* held constant at 0.01 while keeping initial slope constant at 0.0001. *No change* channel type has been kept for consistency.

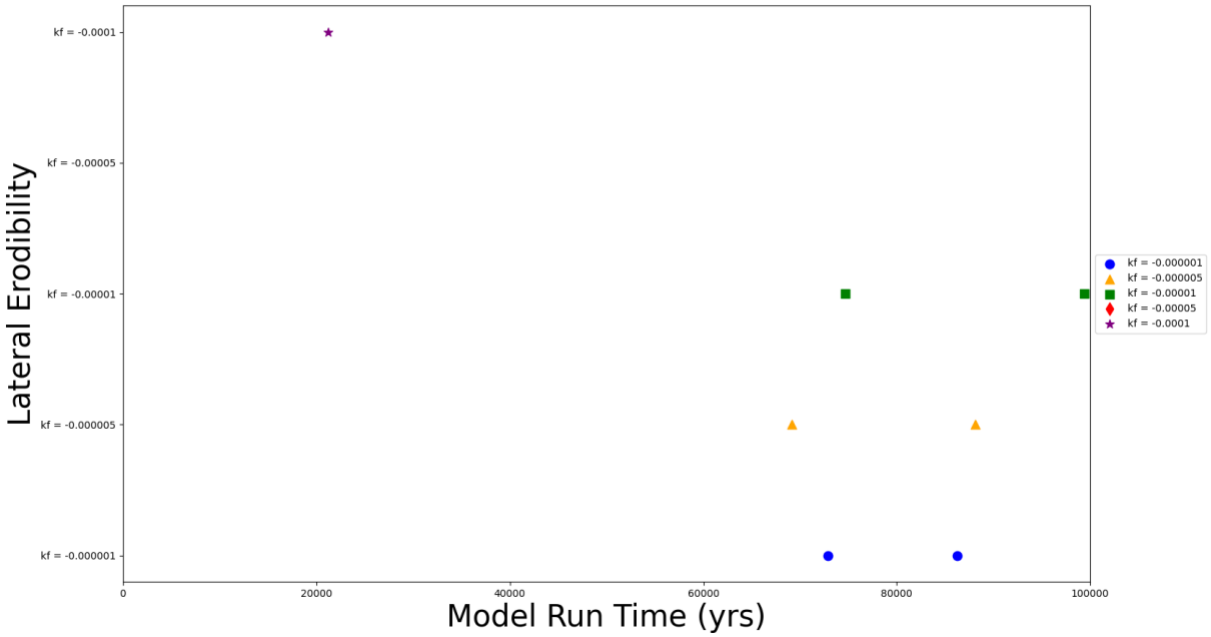

Figure 27. Comparison of cutoff times over 100 ky for different *kf* values. *kl* held constant at 0.01 while keeping initial slope constant at 0.0001. *No change* channel type has been kept for consistency.

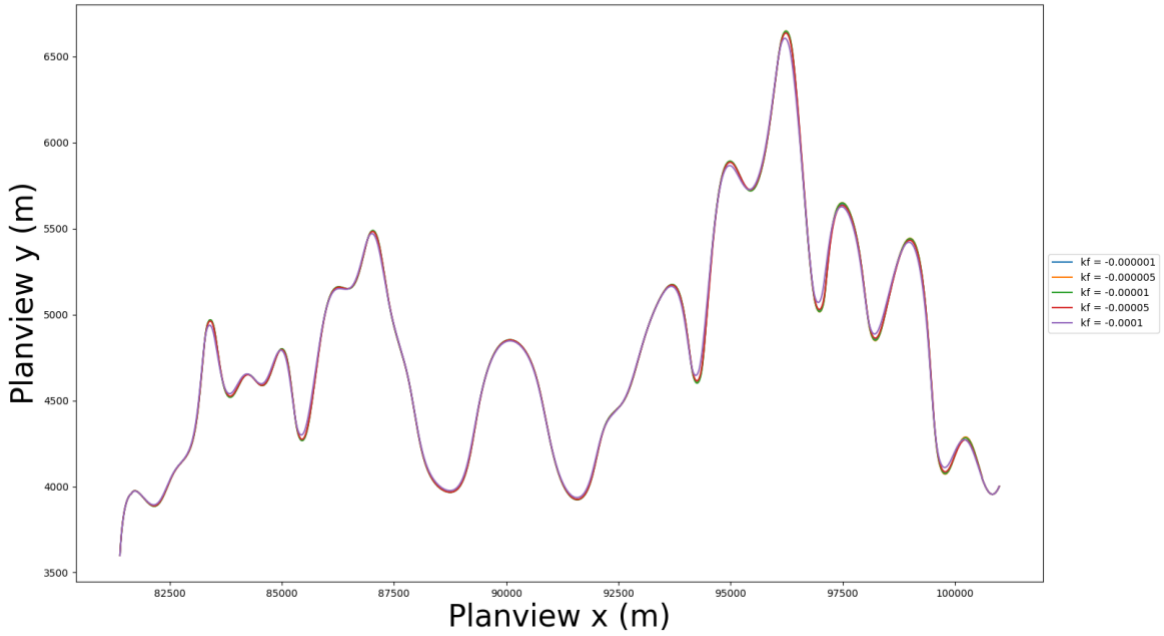

Figure 28. Comparison of planforms at 100 ky for different *kf* values. *kl* held constant at 0.001 while keeping initial slope constant at 0.0001. *No change* channel type has been kept for consistency.

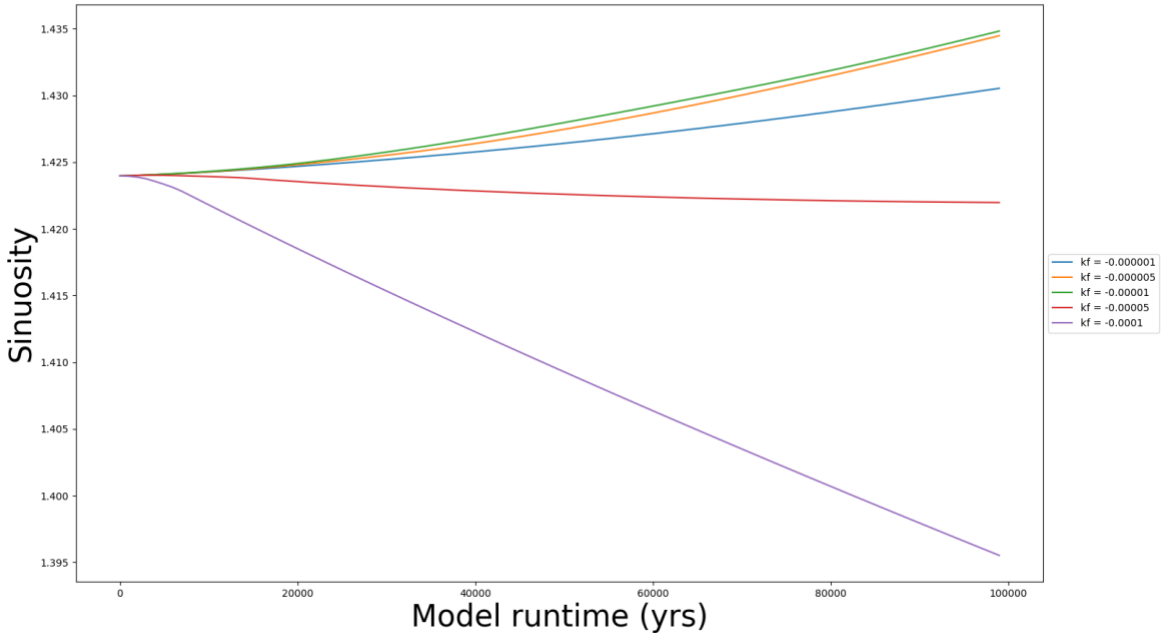

Figure 29. Comparison of sinuosity changes over 100 ky for different *kf* values. *kl* held constant at 0.001 while keeping initial slope constant at 0.0001. *No change* channel type has been kept for consistency.

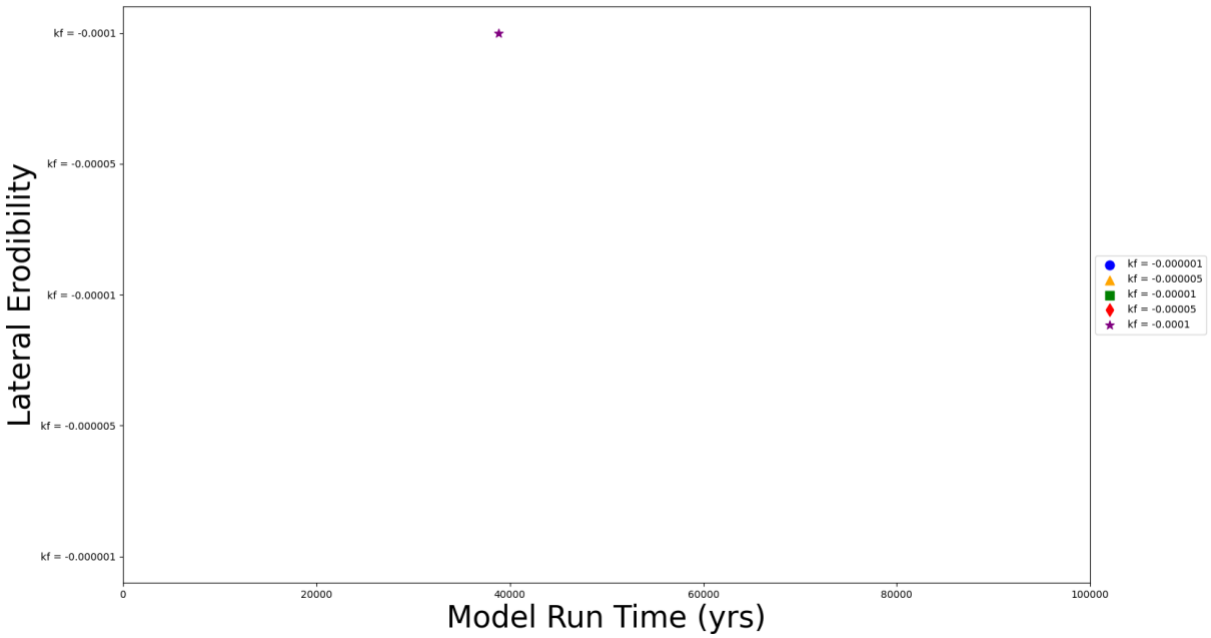

Figure 30. Comparison of cutoff times over 100 ky for different *kf* values. *kl* held constant at 0.005 while keeping initial slope constant at 0.0001. *No change* channel type has been kept for consistency.

Initial Slope

General Trends

Lateral and vertical erodibility values were set to 0.05 and -0.0001, respectively, whereas channel type was still preserved as *no change*. The sole variable investigated is initial slope, which is allowed to vary from 0.005 to 0.00001.

This difference in sinuosity is clear in a plot of sinuosity over time (Figure 31). The sinuosity of the three channels with initial values of 0.005, 0.001, and 0.0005 exhibited an initial increase until 10 to 20 ky, followed by a continuous decrease. Higher initial slopes showed greater and longer lasting increases in sinuosity, with an initial slope of 0.005, the original slope at 16 ky, increasing by 7.0%. In contrast, lower initial slopes of 0.0001, 0.00005, and 0.000001 continuously decreased in sinuosity with time. At 16 ky, the growth in sinuosity was from 1.42 to 1.52; yet by 100 ky, the sinuosity decreased from 1.42 to 1.12.

Changing the values of initial slope seemed to have little effect on the number of cutoffs, although the timing of cutoffs was affected (Figure 32). The initial slope value of 0.005, which is the highest initial slope value in this dataset, had a total of 2 cutoffs. The three lowest initial slope values of 0.0001, 0.00005, and 0.00001 also experienced 2 cutoffs. However, timing of the first cutoff increased from approximately 4,000 to 26,000 model years as the initial slope was increased from 0.00001 to 0.005.

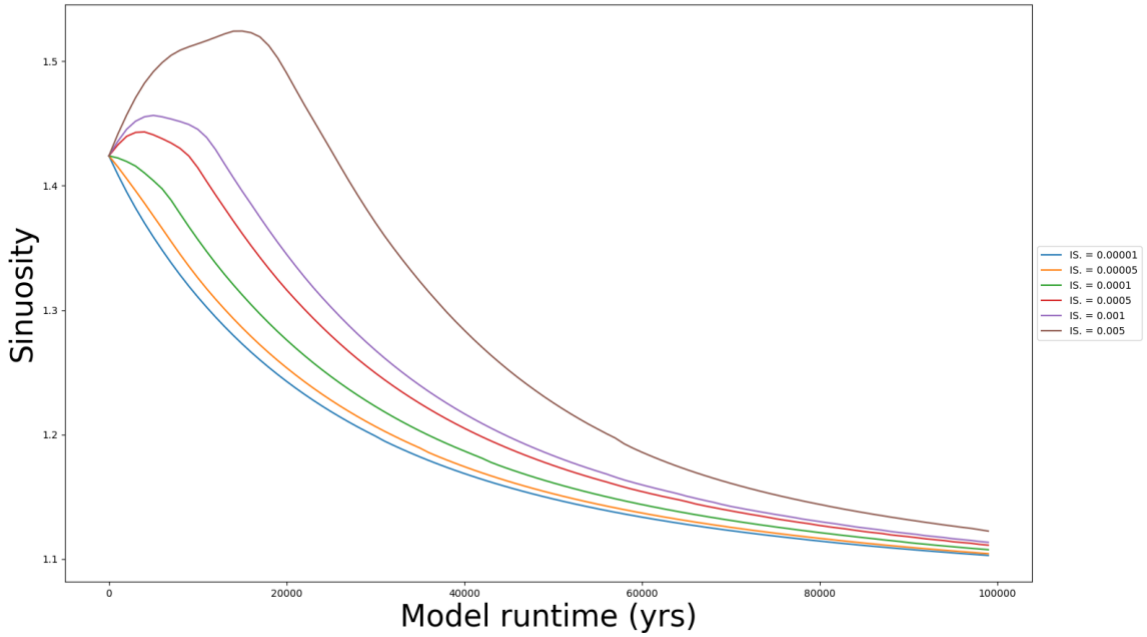

Figure 31. Comparison of sinuosity changes over 100 ky for different initial slope values. *kl* and *kf* held constant at 0.05 and -0.0001, respectively. *No change* channel type has been kept for consistency.

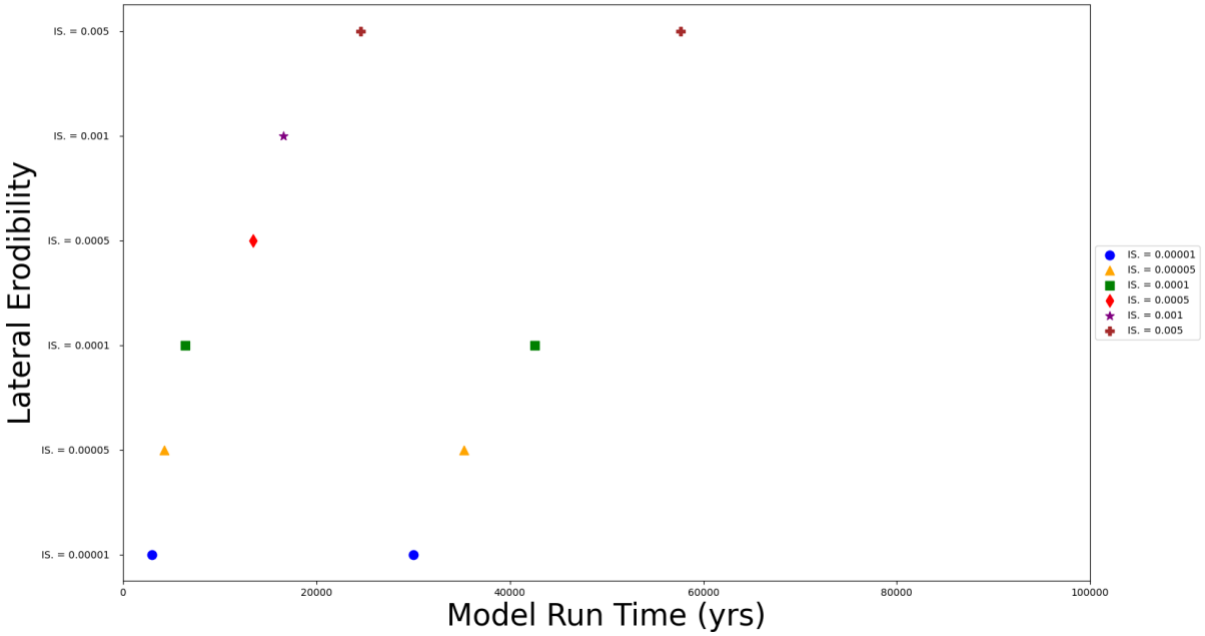

Figure 32. Comparison of cutoff times over 100 ky for different initial slope values. *kl* and *kf* held constant at 0.05 and -0.0001, respectively. *No change* channel type has been kept for consistency.

Channel Geometry

General Trends

Lateral and vertical erodibility and initial slope were held at 0.05, -0.000001, and 0.0001, respectively, while channel geometry was altered to: *no change*, *rectangular*, and *trapezoidal*. The planform for *rectangular* simulations displayed a sinuous loop with a total of 21 meanders, the *no change* channel type showed a total of 16 meanders, and *trapezoidal* simulations showed 4 meanders (Figure 33). The amplitude of the meanders became more variable as the channel geometry grew in complexity; *no change* channel simulations had similar meander amplitudes, whereas the *rectangular* channel types displayed a variety of meander amplitudes. The *trapezoidal* channel type had many small amplitude meanders, although these were within the width of the channel and thus represent braided conditions.

The braided conditions were further inferred by the cutoffs over time (Figure 34). Continuous cutoffs for over 100 ky caused a reduction in sinuosity and resulted in a straighter planform for trapezoidal channels, and the overall instability and dynamism of the channels were recorded in the frequent cutoffs and the average sinuosity of 1.2, which is well below the common threshold of 1.5 for meandering channels (Figure 35).

The *rectangular* and *trapezoidal* channel frequently experienced cutoffs, and their sinuosity values also exhibited periodic oscillation, with values alternately increasing and decreasing over time. In contrast, the *no change* channel linearly increased its sinuosity with little cutoffs. The *trapezoidal* channel decreased its sinuosity from 1.42 to 1.29, or by 9.2%.

Conversely, both the *rectangular* and *no change* simulations showed channels that increase their sinuosity to 1.88 and 1.99 by 32.4% and 40.1%, respectively (Figure 35).

The difference in cutoff frequency was even more pronounced in the number of cutoffs over time. When the channel geometry was *rectangular*, it experienced 122 cutoffs in the 100 ky simulation. However, the *trapezoidal* channel geometry resulted in 783 cutoffs, compared to only six cutoffs in the case of the *no change* channel (Figure 34).

These strongly dissimilar behaviors between channel geometries were dependent on the erodibility values simulated. When *kl* and *kf* were assigned different values of 0.01 and -0.00005, correspondingly, for *no change*, *rectangular*, and *trapezoidal* simulations, the three channel geometries showed a high degree of correlation with each other in planforms (Figure 36). The sinuosity values over 100 ky also demonstrated a consistently linear minor increase with the *no change* simulation increasing the least, to 1.44 or by 1.4%; the *trapezoidal* increasing to 1.47 or by 3.52%; and the *rectangular* increasing the most, to 1.48 or by 4.2% (Figure 37). The *rectangular* channel type underwent one cutoff at ~78 ky, while the other two types did not experience any cutoffs over the 100 ky period (Figure 38).

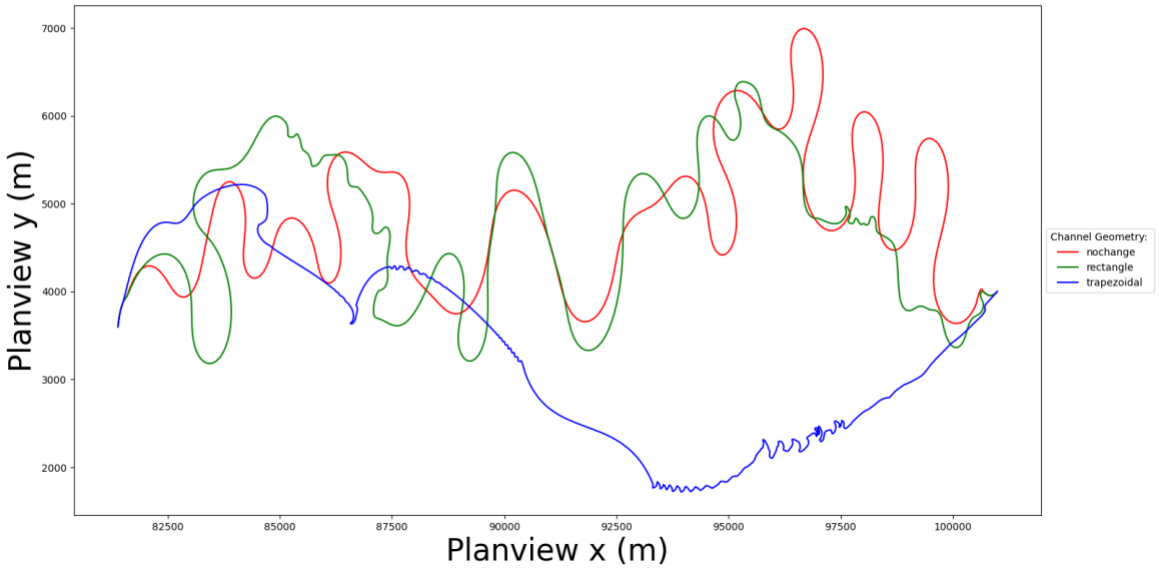

Figure 33. Comparison of planforms at 100 ky for different channel types: *no change*, *rectangular*, and *trapezoidal*. *kl*, *kf*, and initial slope held constant at 0.05, -0.000001, and 0.0001, respectively.

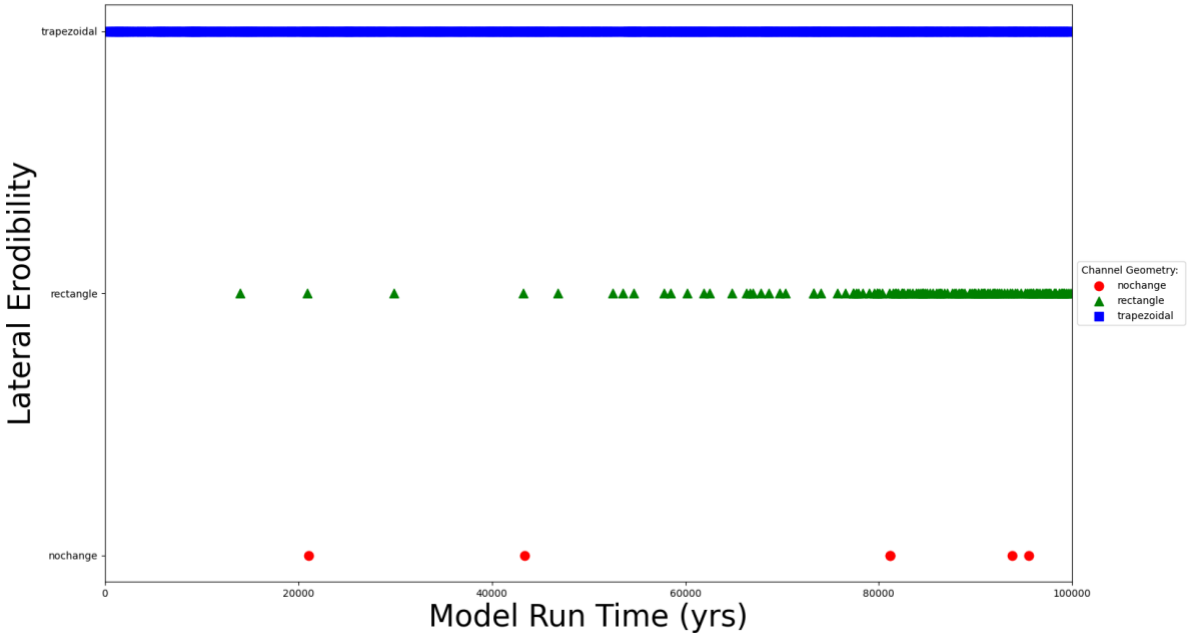

Figure 34. Comparison of cutoff times over 100 ky for different channel types: *no change*, *rectangular*, and *trapezoidal*. *kl*, *kf*, and initial slope held constant at 0.05, -0.000001, and 0.0001, respectively.

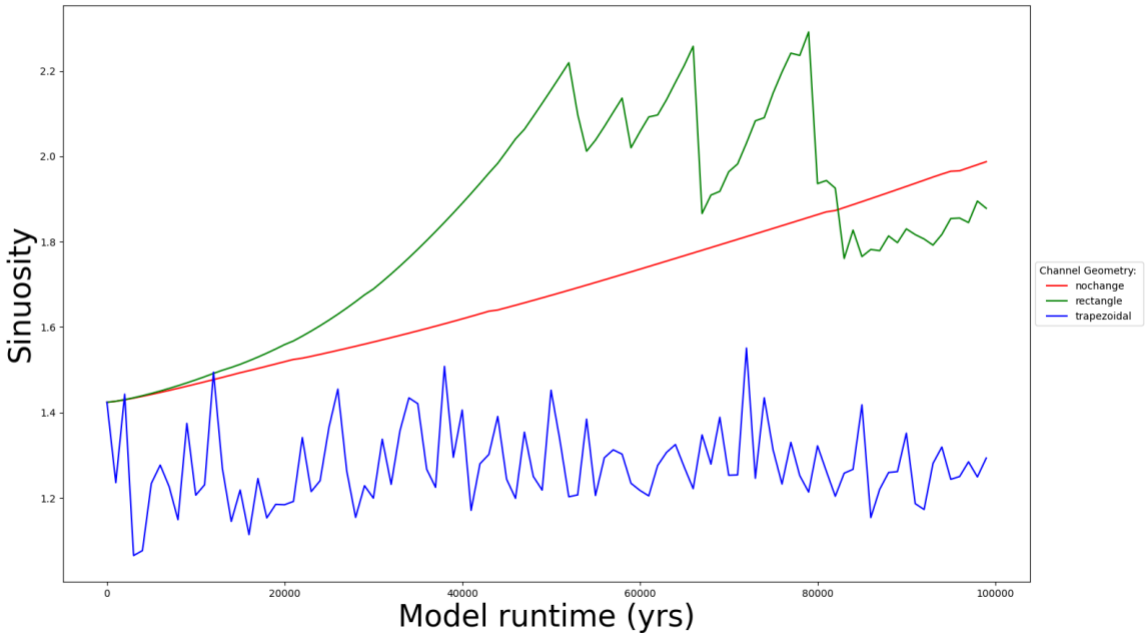

Figure 35. Comparison of sinuosity changes over 100 ky for different channel types: *no change*, *rectangular*, and *trapezoidal*. *kl*, *kf*, and initial slope held constant at 0.05, -0.000001, and 0.0001, respectively.

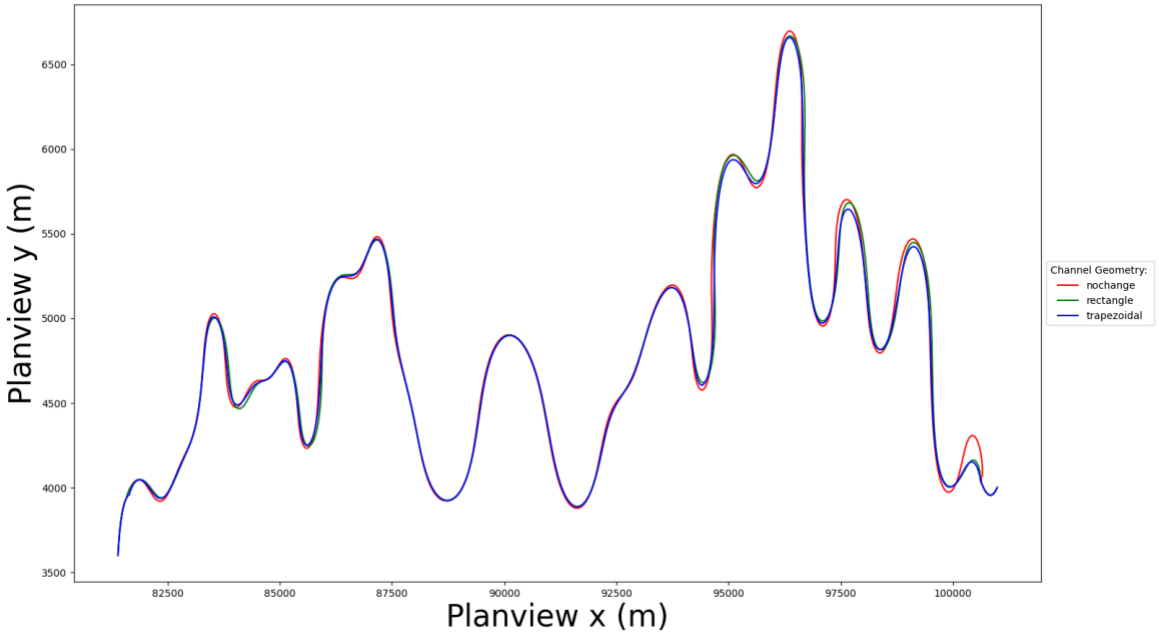

Figure 36. Comparison of planforms at 100 ky for different channel types: *no change*, *rectangular*, and *trapezoidal*. *kl*, *kf*, and initial slope held constant at 0.01, -0.00005, and 0.0001, respectively.

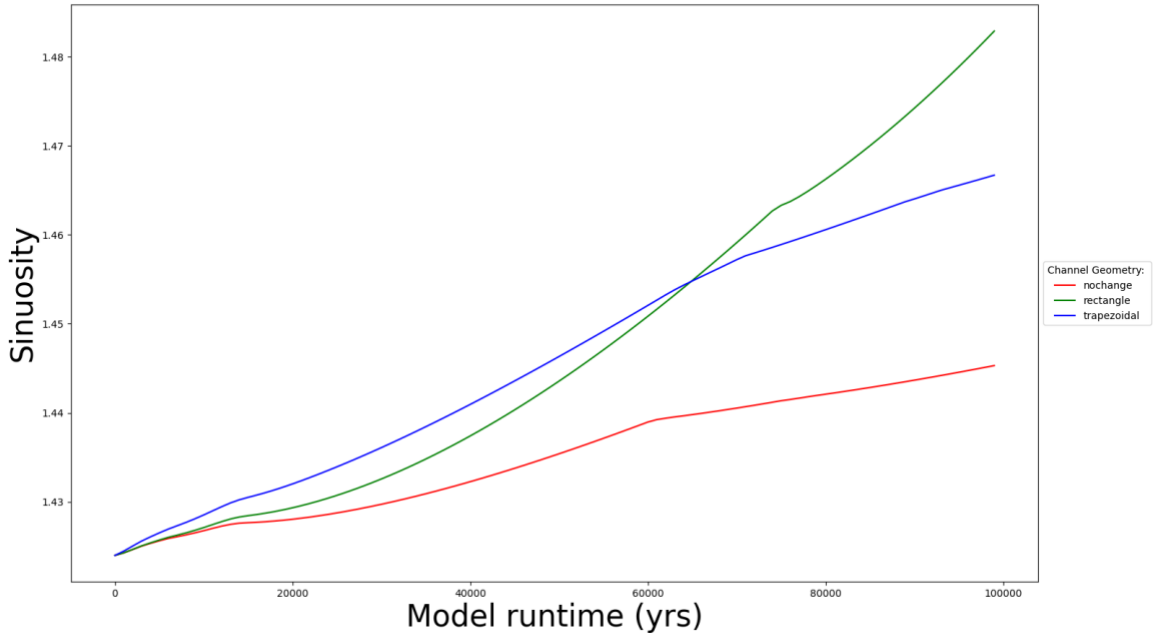

Figure 37. Comparison of sinuosity changes over 100 ky for different channel types: *no change*, *rectangular*, and *trapezoidal*. *kl*, *kf*, and initial slope held constant at 0.01, -0.00005, and 0.0001, respectively.

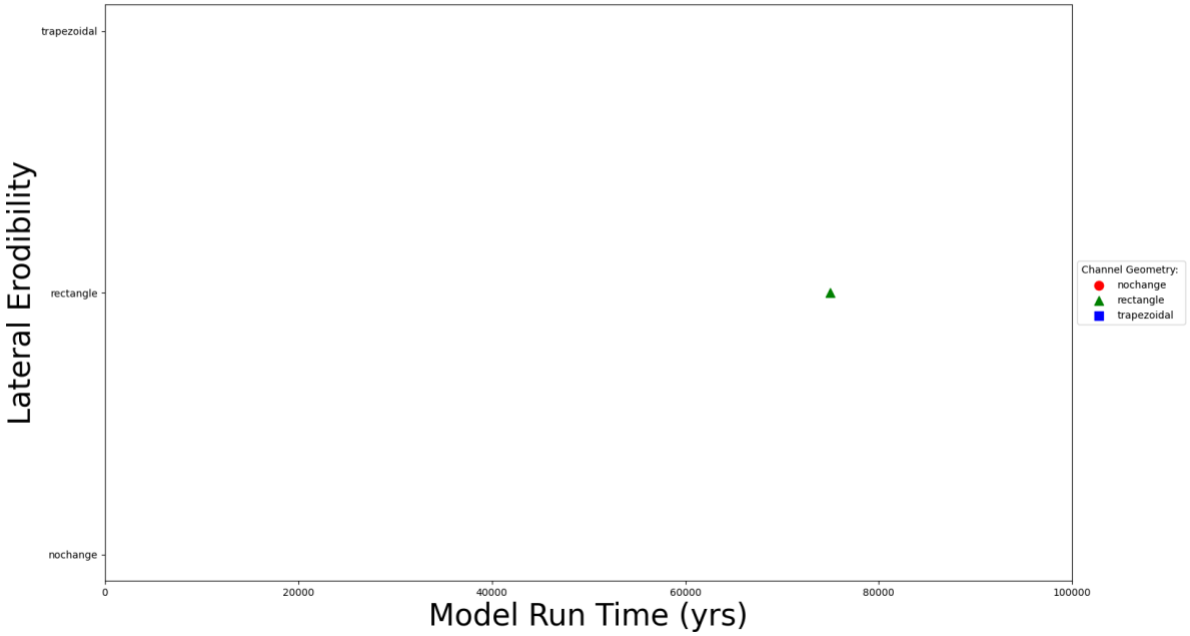

Figure 38. Comparison of cutoff times over 100 ky for different channel types: *no change*, *rectangular*, and *trapezoidal*. *kl*, *kf*, and initial slope held constant at 0.01, -0.00005, and 0.0001, respectively.

Lithologic Anisotropy

General Trends

In this section, I analyzed how the ratio of lateral to vertical erodibilities, which dictates the lithologic strength anisotropy, influences the sinuosity change. This analysis was done for all three channel types, holding initial slope constant at 0.0001.

For *no change* and *rectangular* channel types, increasing the value of *kl* led to more noticeable changes in sinuosity than comparable increases in *kf* do (Figures 39, 40). The runs with *kl* = 0.1 consistently exhibited the most substantial increase in sinuosity, followed by 0.05, while the remaining three values, 0.01, 0.005, and 0.001, showed the least change in sinuosity, sequentially. This pattern held true across all *kf* values and indicated that when the values of *kf* and initial slope were kept constant, a cutoff was less likely to occur if the *kl* value was too small. For example, if the *kl* value was 0.001, simulations across all *kf* values and channel types displayed only minor sinuosity change over 100 ky, and all these values experienced no cutoffs. On the other hand, a higher value of *kl* resulted in more cutoffs, although the relationship between the two was neither linear nor quadratic. For example, although a *kf* value of -0.000005 is greater than a *kf* value of -0.000001, the former still experienced seven more cutoffs for kl value of 0.1.

For *kl* values of 0.1 and 0.05 (the largest *kl* values in the dataset) with either *no change* or *rectangular* channel types, the channel planforms appeared straight when assigned a *kf* value of -0.0001 (the highest *kf* in the dataset) (Figures 39, 40). As smaller *kf* values were applied, the

planforms became more sinuous. When the *kf* value is -0.000001, the *no change* and *rectangular* channels increased their final sinuosity to 2.67 and 1.96, respectively, or by 88.7% and 38.0%, respectively. All the comparisons of sinuosity over time indicated that the sinuosity of the *kf* value -0.0001 decreased, while the sinuosity of the remaining four *kf* values increased over 100 ky. The degree of decreasing sinuosity for *kf* = -0.0001 was dependent on the lateral erodibility value. With a *kl* value of 0.05, the sinuosity decreased to 1.10, representing a 22.5% reduction. However, if the *kl* value was smaller, such as 0.01, the final sinuosity was only reduced to 1.25 (by 12%). Therefore, the highest *kf* value, representing rock types that have high vertical erosion potential, caused threshold behavior, and, when paired with lateral erosivity, indicated that high lateral and vertical erosivity leads to unstable meandering and formation of straight channels.

Exceptions

There is an exception where *kf* values of -0.00005 led to a decreasing trend, when the *kl* value was 0.001, which was the smallest value analyzed in the simulations. However, the reduction in sinuosity was relatively small for *kf* values of -0.00005, with a decrease from 1.4239 to 1.4219 (a reduction of 0.14%) for the *no change* channel type and a decrease from 1.4240 to 1.4223 (a reduction of -0.12%) for the *rectangular*.

Whereas the lithologic anisotropy represented by the *kl* and *kf* ratios resulted in similar behavior for *rectangular* and *no change* channels, the *trapezoidal* channel type behaved dissimilarly. Decreasing sinuosity occured in several simulations, and not just when *kf* was high (Figure 41). Generally, when lateral erodibility is high, the simulations increase in sinuosity or become more meandering, except for high *kf* values. This, and the lowest *kl* value, are the only ones that follow the *rectangular* and *no change* trends. For the second highest *kl* value, no

significant change in channel sinuosity occurs until the two highest lateral erodibilities; here the highest lateral erodibility increased sinuosity, whereas the second highest decreased it. The medium lateral erodibility simulated (kl = 0.01) had no consistent trend with vertical erodibility and alternated between increasing and decreasing sinuosities. Overall, it is harder to predict channel behavior for trapezoidal channel types.

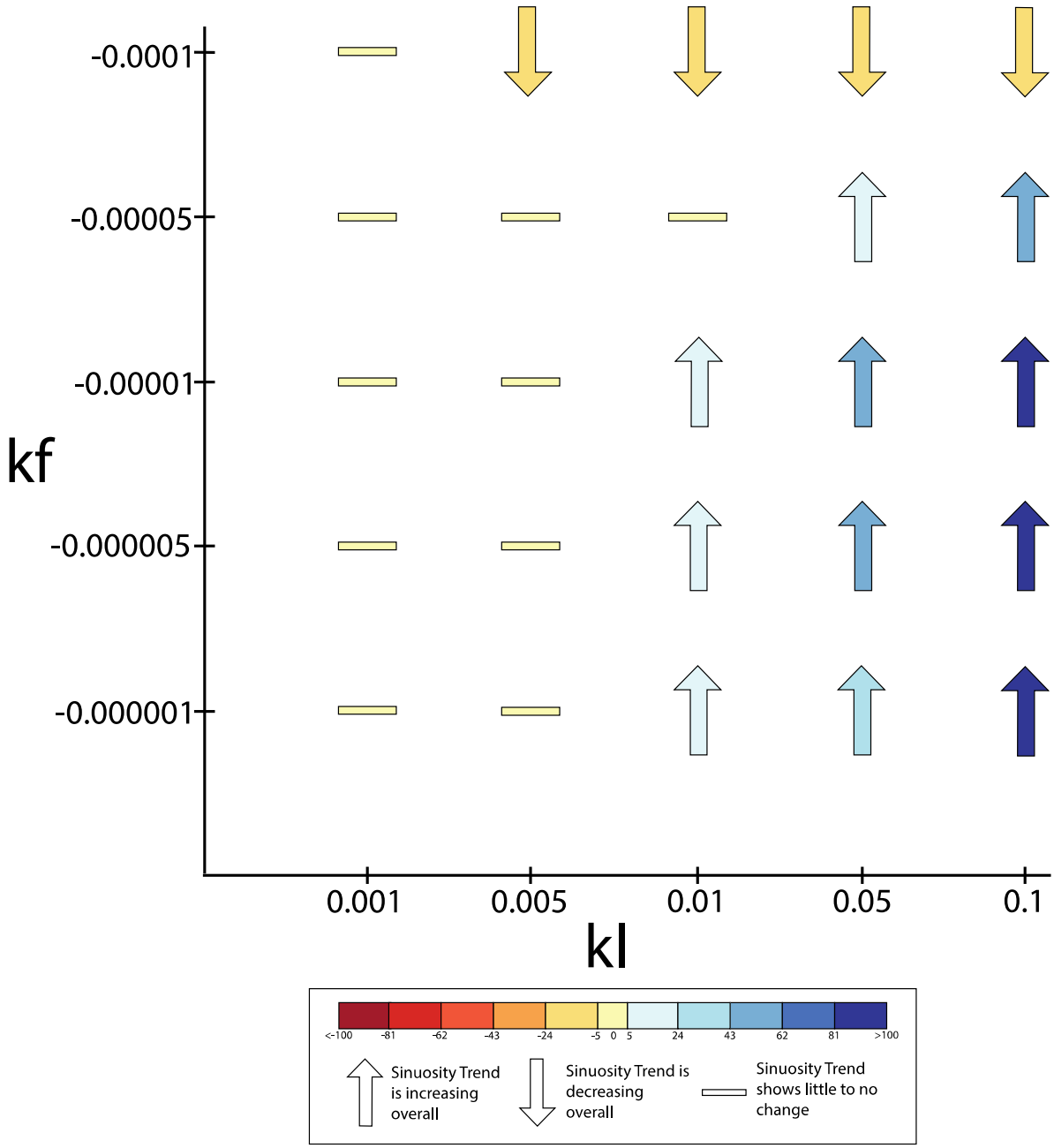

Figure 39. The overall sinuosity pattern of simulated river channels that has a lateral erodibility from -0.000001 to -0.0001, vertical erodibility from 0.001 to 0.1, and a fixed initial slope of 0.0001 with a *no change* channel type.

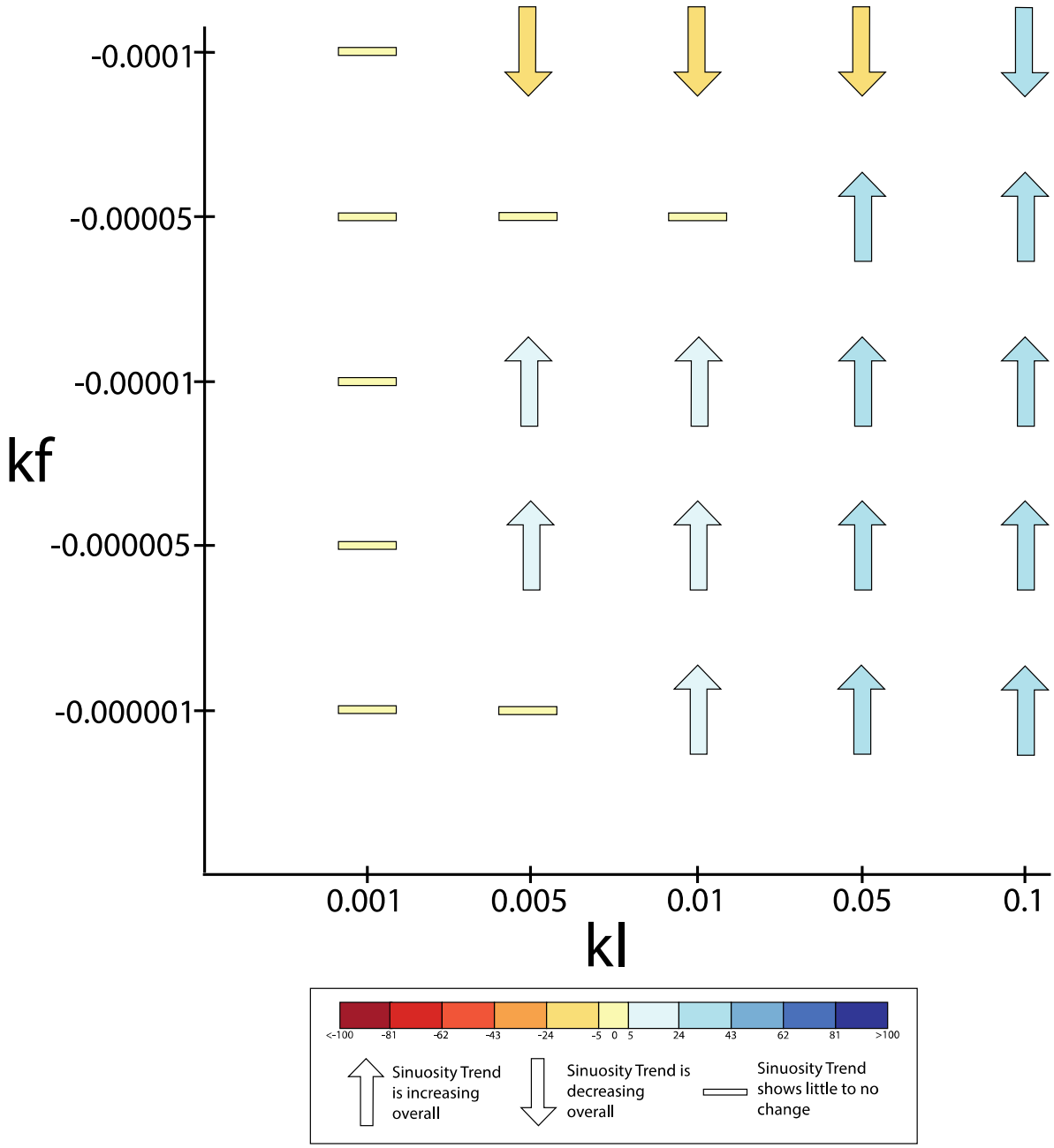

Figure 40. The overall sinuosity pattern of simulated river channels that has a lateral erodibility from -0.000001 to -0.0001, vertical erodibility from 0.001 to 0.1, and a fixed initial slope of 0.0001 with a *rectangular* channel type.

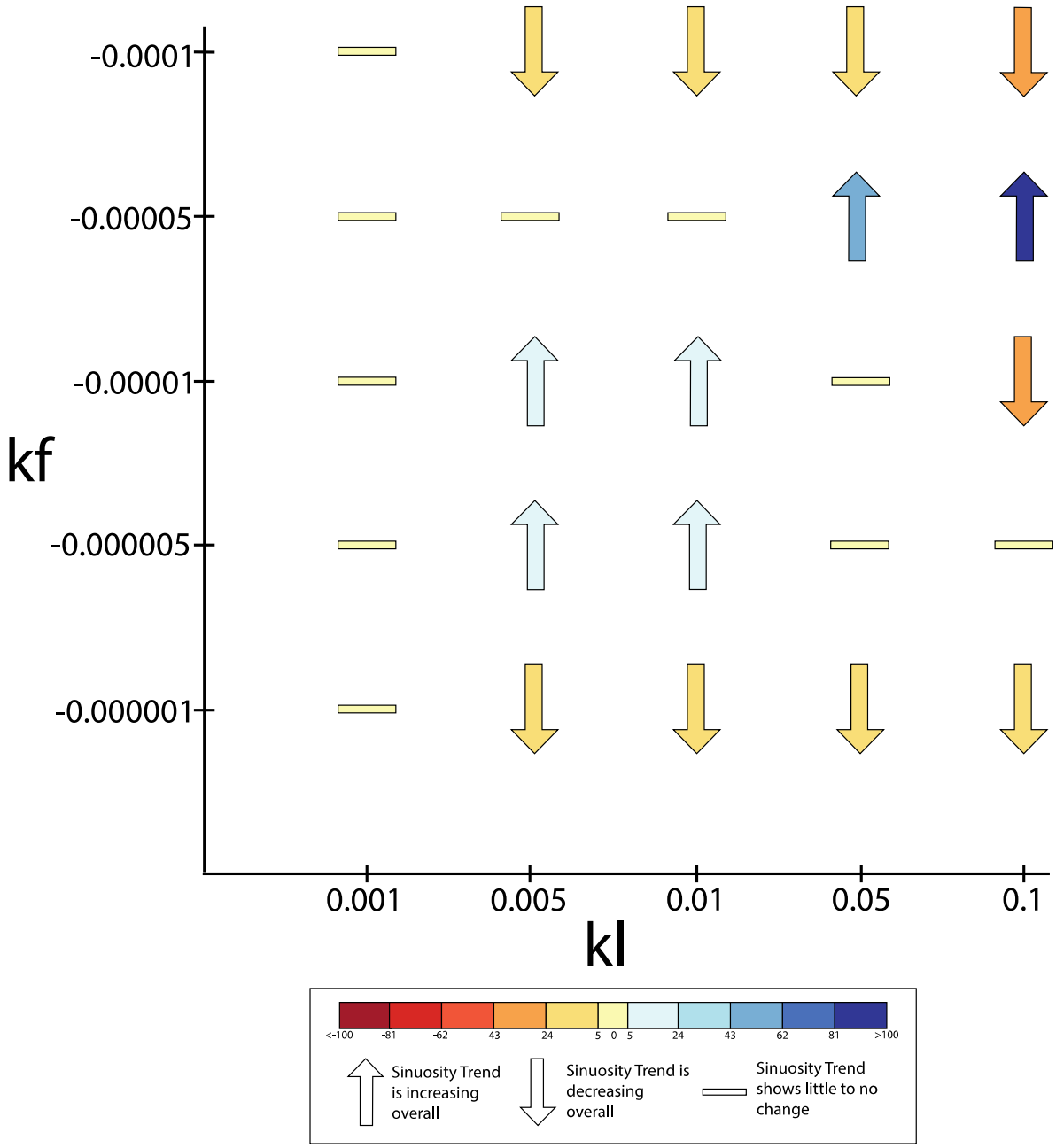

Figure 41. The overall sinuosity pattern of simulated river channels that has a lateral erodibility from -0.000001 to -0.0001, vertical erodibility from 0.001 to 0.1, and a fixed initial slope of 0.0001 with a *trapezoidal* channel type.

DISCUSSION

Initial Slope

Except for the highest initial slope value with a rectangular channel type, the trends for all initial slope values across different channel types behaved similarly in that they all displayed an overall decreasing sinuosity over time with very few cutoffs. Channels with higher initial slope values increase their sinuosity at the beginning of the simulation. They also show more long-lasting sinuosity increases before transition to a decreasing trend; the rate of sinuosity decrease is higher. resulting in nearly the same sinuosity value as that of lower initial slope values by 100 ky. This initial increase in sinuosity at higher slopes seems counter-intuitive, as field observation tend to show higher sinuosity channels in low slope environment.

However, tracing the mathematical relationships reveals why a higher slope initially results in a more sinuous channel. When the initial slope of a channel increases, the calculated water height decreases to balance Manning's equation for a set discharge and channel width. The reduced water height in turn decreases the weighting factor in the calculation of lateral migration rate and lowers the impact of upstream nodes on migration (Howard & Knutson, 1984). This means that channel nodes with high curvature will experience higher migration rates because the influence of low curvature nodes upstream is lower in simulations with high slope and low water height. However, sinuosity decreases because of a negative feedback; higher slopes cause increased basal shear stress and vertical erosion rates, causing the channel profile to vertically erode and decrease slope. The lowered slope then causes an increase in water height and an

increase in the impact of upstream nodes on migration rates. Thus, the higher initial slope has only a temporary effect on lateral migration in the models.

According to field observations, rivers tend to have higher sinuosity in low slope environments, while an increase in slope typically results in a decrease in meandering (Yanites et al., 2013; Allen et al., 2013; Mitchell and Yanites, 2021). Many studies have shown that meander migration rates can be altered when a river passes through multiple lithologies or tectonic zones, and meandering patterns can be affected as a result. Yanites et al. (2013) conducted field observations and collected data on channel width, depth, and slope, as well as sediment characteristics and geological context, along the Peikang River in central Taiwan, which runs through multiple lithologic zones and is actively deformed by faults. The study found that narrower channels tend to have steeper slopes and deeper incisions, whereas wider channels tend to have gentler slopes and shallower incisions. Observations from ten river channels located in the Mohand range of the Siwalik Hills in northwest India indicate that the increase in rock strength promotes the development of meandering patterns in river channels by narrowing them and enhancing lateral erosion (Allen et al., 2013). Mitchell and Yanites, (2021) employed an approach that utilizes stream steepness, a known base level fall rate, and contact dips, combined with previous work on erodibility values of mixed lithologies. They discovered that in the context of bedrock rivers that cut through layered rock formations, differences in rock strength between different layers can impact various aspects of the river's behavior. For instance, such contrasts can affect the slopes of the river channel, the rates at which erosion occurs, and the speed at which kinematic waves propagate along the river profile. These field observations contradict my model simulations from initial slope. However, dynamic width (Yanites, 2018), a key mechanism which allows channel width to adjust in response to slope, is missing in the

model. Once this is implemented, water height will be less sensitive to slope changes and so the weighting function for lateral migration—and thus sinuosity changes—will not react in a manner that is counter to field observations. Dynamic width is currently being added to the meander model, and my results highlight the necessity of this mechanism for the simulated bedrock rivers to behave similarly to field observations when slope is adjusted.

Channel Geometry

Across all the channels with distinct lateral and vertical erodibility values, the *no change* and *rectangular* channel types behave similarly. When all variables but channel geometry are held similar, simulated channels display a comparable temporal pattern in sinuosity and planform geometry. The large number of cutoffs in the *rectangular* channel type simulations exert a small influence on sinuosity, with an overall increase in sinuosity through time, whereas cutoffs in the *trapezoidal* simulations tend to decrease sinuosity substantially. Notably, the behavior of the *trapezoidal* channel type differs from that of the *no change* and *rectangular* channels as seen in the opposing sinuosity with time trends and the distinct planforms that develop.

Numerically, the *trapezoidal* channel differs in that it directly incorporates the vertical incision history of the channel at each node. The width and height of the *trapezoidal* channel type will grow with greater lateral and vertical erosion rates, meaning that the channel is constantly adjusting its geometry. In comparison with the *trapezoidal* channel type, the *rectangular* channel type only grows in width with lateral erosion, and *no change* channel type maintains a constant width and height.

Cutbank erosion in our simulated meandering bedrock channels is believed to be weathering limited. This phenomenon has been suggested by Johnson and Finnegan (2011), who

suggest that in these channels point bar deposition and cutbank erosion are asymmetric when compared to meandering alluvial channels. Consequently, little negative feedback is exerted on cutbank erosion in a meandering bedrock channel, and braiding in an actively meandering bedrock river canyon can begin at bends where erosion on the outer bank has widened the channel beyond the point of meandering stability and into the regime of braiding stability (Finnegan and Balco, 2013). Another way for a channel to initiate braiding is when a channel becomes wide enough that a chute cutoff occurs on the inside of point bars (Ashmore, 1991; Carson, 1984), which redirects the flow over the point bar and raises the water level upstream of the chute (Ashmore, 1982). The *rectangular* model follows the proposed endmember in Finnegan and Balco (2013) whereby bedrock channels cannot reform banks and grow laterally until they are unstable enough to initiate braiding. However, the simulated channels experienced many cutoffs under different lateral migration rates but still maintained a stable meandering state, indicating that the proposed meandering–braiding cycles in Finnegan and Balco (2013) either do not take place or take at time scales greater than 100 ky.

Erodibility

The simulations consistently show that, regardless of the channel geometry, the combination of high vertical erodibility and any level of lateral erodibility leads to a decreasing trend in sinuosity over time with few channel cutoffs. Theoretically, this observation makes sense because a river's ability to meander, with a winding, snake-like pattern of the channel, can be limited by high vertical erosion. This is because when the channel is subject to high vertical erosion, it becomes narrower and deeper, with steep banks and a relatively straighter path, which makes it more difficult to erode the banks of the channel and form meanders. As a result, the

river may be less able to meander and to form bends in its course. As a further consequence, there would be fewer cutoffs due to the direct response of losing the capacity for the channel to migrate.

Numerically, the model relates vertical erodibility and meandering through the slope adjustment. As vertical erodibility increases, the same basal shear stress will result in higher rates of vertical erosion, which decreases channel slope. As channel slope decreases, the water depth increases following the relationships in Manning's equation for a constant discharge and channel width. The increased water depth then increases the weighting function for upstream nodes set by Howard and Knutson (1984), and decreases the effective lateral migration rate. This lowers the sinuosity.

As the lateral erodibility or *kl* value increase in simulations, sinuosity trends display a greater variability, and tend to produce more cutoffs. Numerically, this is supported because as *kl* increases, the same local curvature will result in a higher predicted lateral migration rate and thus a higher sinuosity. As sinuosity increases, the potential for cutoffs will also increase due to the changing channel positions.

Bedrock that has a high lateral erodibility value and is prone to slaking exhibit greater curvature and sinuosity. Johnson and Finnegan (2015) investigated two bedrock channels located in the Santa Cruz Mountains of California, namely Pescadero Creek, which has a mudstone bedrock, and Butano Creek, which has a sandstone bedrock. Both the field and lab observations show that mudstone undergoes disintegration after being wet and then drying, while sandstone maintains its tensile strength, even after undergoing the same process (Johnson and Finnegan, 2015). These observations provide insights into the morphology of the two rivers, as Pescadero

Creek exhibits active meandering and sinuosity, while Butano Creek has a straight to sinuous channel (Johnson and Finnegan, 2015).

Typically, when the rates of vertical erosion are significantly higher, resulting in intense incision of the channel bed, the river channel tends to exhibit less sinuosity compared to a channel with lower vertical erosion rates (Johnson and Finnegan 2015; Stark et al., 2010). However, this relationship may not hold true if both the rates of wall erosion and bed erosion are high. This is because, numerically, horizontal channel erosion rates are more responsive to variations in rock erodibility compared to vertical channel erosion rates. In such cases, the river channel may exhibit a significant increase in sinuosity, resulting in the formation of an incised meandering river (Johnson and Finnegan 2015; Stark et al., 2010; Finnegan and Dietrich, 2011).

Lithologic Anisotropy

There are three general patterns that emerged from different combinations of parameters in the numerical model: 1) stable meandering, in which increasing lateral erodibility values leads to more cutoffs, but the channel still has an increased sinuosity; 2) straight channels with a very high vertical erodibility value, yet the channel shows a decreasing trend in sinuosity with few cutoffs; and 3) braided channels in which a channel experienced too many cutoffs to maintain meander stability, causing the sinuosity to decrease, and annual cutoffs occur on high frequency/low amplitude meanders.

Initially, all the simulated channels start off displaying a sinuous pattern, but because of different rock types with distinct lateral and vertical erodibility, they behave differently and eventually end up transitioning into a unique channel pattern. Strath terrace formation can provide valuable insights into the influence of weathering processes on bedrock rivers

(Montgomery, 2004). In general, strath terraces are more extensive in rivers that flow over weak sedimentary rock, and they tend to be less developed or preserved in rivers that flow over hard and erosion resistant rock (Montgomery, 2004). This suggests that the nature of the underlying bedrock plays a significant role in the formation and preservation of strath terraces, emphasizing the importance of weathering processes in shaping river landscapes (Montgomery, 2004). In rocks with low lateral erodibility, terraces may not form due to the lack of lateral migration, like straight channels with a relatively large vertically erodible force and/or small horizontal migration rate. On the other hand, rivers in rocks with high lateral erodibility or slaking behavior are more likely to form terraces because they can undergo stable meandering and lateral migration, which contributes to the formation of terraces. Terraces in river landscapes can therefore be used to infer the role of underlying bedrock and various weathering processes. Strath terraces formed previously by bedrock channels can also exhibit preserved periods of braiding, like a terrace at Arroyo Seco, NM, which indicated that a section of the river once had a braided channel (Finnegan and Balco, 2013). When single-thread channels experience high lateral migration rates, excessive cutoffs can occur, causing the channels to become unsustainable and transitioning into a multi-thread channel that struggles to maintain meander stability.

Although it will be very difficult to correlate physical rock type with corresponding vertical and lateral erodibility values, some patterns described above can help distinguish and estimate some common behaviors in the evolutional patterns of meandering rivers. Accretionary complex lithologies tend to host the most sinuous incising rivers, as these rocks are typically low in strength and highly erodible, consisting mainly of silt and fine sand turbidites with intermittent coarser, stronger units (Stark et al., 2010). Channels incised into these rocks are known for their

high degree of meandering and their ability to maintain their stability due to a balanced ratio of vertical and lateral erodibility. This balanced erosion process allows sinuous rivers to maintain their stability over time, as the channel adjusts and evolves in response to changes in water flow, sediment transport, and other environmental factors. My simulations reflect these field observations. Models with high lateral erodibility increased their sinuosity over the 100 ky and showcased stable meandering behavior.

The least sinuous single thread incising rivers are typically found in generally erosion-resistant non-alkali mafic volcanics, which encompass a range of rock strengths, from very strong fresh basaltic lavas to weathered, unwelded, and much weaker tuffs (Stark et al., 2010). The substrates of these river channels have higher vertical erodibility than lateral erodibility, which can result in rapid incision of the river channel. This means that the underlying bedrock or sediment of the river channel can be easily eroded vertically, leading to river downcutting and deepening of the channel over time. This aligns with my simulation results, which generated channels with high vertical erodibility values.

When the lateral erodibility value is relatively large compared to the vertical erodibility value due to cyclic wetting and drying cycles (Montgomery, 2004), it can lead to instability in the channel, potentially resulting in channel avulsion or bank failures that disrupt the overall channel stability. In my simulations, I observed that channels with trapezoidal channel types and frequent cutoffs led to constant migration of the channel from its previous position. While the mode only represented a single-thread river channel, it was evident that jagged meander loops indicated multi-thread channel behavior with high lateral erodibility.

Smith River

Comparison of the characteristics of a real-world river reach with simulated river channels allows for a more robust evaluation of the model's performance, its ability to accurately replicate real-world river dynamics, and provides additional evidence for its reliability and credibility. The study area of the Smith River has historically been characterized as a single-thread, sinuous bedrock river that flows predominantly over arkosic sandstone and siltstone from the Tyee Formation (Walker and Duncan, 1989; Walker and MacLeod, 1991). The primary influence on the study area is the lithology, and plays a significant role in shaping the geomorphology, hydrology, and ecological dynamics of the area. The study area of the Smith River aligns with the simulated river channels that exhibit a balanced ratio of lateral and vertical erosion rates. It showed characteristics of initially meandering river channels that gradually increased sinuosity, maintained stability, and continued to exhibit meandering patterns, thus indicating that the simulated river channels accurately replicate this characteristic of natural river systems.

Further comparison with the Smith River will be possible when geochronologic data collected by myself and the Schanz/Yanites research team is made available. These cosmogenic radionuclide and optically stimulated luminescence dates will quantify the vertical and lateral erosion rates along the Smith River over the last 100 ky, and provide information about the variability in sediment supply through time. With these data, one can start to compare the model directly and quantitatively with the Smith River.

CONCLUSION

I used a numerical model that is developed by Profs Sarah Schanz and Brian Yanites to specifically test the sensitivity of bedrock meandering development to lithologic strength differences. Each model run starts off from a single thread meandering bedrock river. The model is run for 100,000 model years using Indiana University's supercomputer. Specific variables such as lateral erodibility, vertical erodibility, initial slope, and channel geometry are held constant individually to perform sensitivity analyses. The data collected from the supercomputer is then processed to examine the stability and growth of each simulated meandering river. The effects of those specific variables are then visualized and compared for the analysis of evolutionary patterns.

The three evolution patterns of a single-thread meandering bedrock river can be summarized as follows:

1. Straight Channel: This pattern is characterized by a highly erodible force that incises the river channel, reducing its sinuosity. It is primarily controlled by high vertical erodibility, resulting in straightening of the channels, with reduced meander bends.
2. Meandering Channel: Despite experiencing many cutoffs, the channels in this pattern remain single thread and meandering due to high lateral erodibility. The subtle balance between lateral and vertical erodibility may cause channels to briefly initiate braiding but still maintain a meandering pattern.
3. Braided Channel: In this pattern, the river channel becomes multi-threaded and constantly migrates, with frequent cutoffs due to high lateral erosion rates. This can cause the channels to lose their meander stability and transition into a multi-threaded, braided

pattern. This is caused by creating asymmetric channels whose width and depth evolve in response to vertical and lateral erosion rates.

A single thread meandering bedrock river can evolve into a straight channel, meandering channel, or transit to exhibit braided patterns, depending on the balance between lateral and vertical erosion rate and the geometry of the river channel.

The characteristics of a reach of a real-world river, the Smith River, are compared with the simulated river channel. This provides direct field evidence that further supports the behavior of the model.

For the future work, lithologic controlled erosion style is a variable that I want to include in the model. It can reflect rock erodibility properties and predicts how sediment will erode the underlying bedrock and allows for simulation of abrasion-dominated erosion, which commonly occurs in homogeneous crystalline rock (Whipple et al., 2000) or weathering-dominated erosion, which commonly occurs in slaking-prone sandstone (Schanz and Montgomery, 2016). Unfortunately, this requires the model to be able to calculate sediment flux efficiently, which is not expected to be ready until mid-Fall 2023.

REFERENCES

Allen, G. H., Barnes, J. B., Pavelsky, T. M., & Kirby, E. (2013). Lithologic and tectonic controls on bedrock channel form at the northwest Himalayan front: BEDROCK CHANNEL FORM, MOHAND, INDIA. *Journal of Geophysical Research: Earth Surface*, v. *118*(3), p. 1806–1825. https://doi.org/10.1002/jgrf.20113.

Ashmore, P. E. (1991). How do gravel-bed rivers braid? *Canadian Journal of Earth Sciences*, v. *28*(3), p. 326–341. https://doi.org/10.1139/e91-030.

Ashmore, P.E. (1982). Laboratory modelling of gravel braided stream morphology. *Earth Surface Processes and Landforms*, v.7, p. 201-205.

Baldwin, E.M., (1956). Geologic map of the lower Siuslaw River Area, Oregon: U.S. Geological Survey Oil and Gas Investigations Map OM-186, 1 sheet, scale 1:62,500.

Bender, A. M., Amos, C. B., Bierman, P., Rood, D. H., Staisch, L., Kelsey, H., & Sherrod, B. (2016). Differential uplift and incision of the Yakima River terraces, central Washington State. *Journal of Geophysical Research: Solid Earth*, v. *121*(1), p.365–384. https://doi.org/10.1002/2015JB012303.

Bursztyn, N., Pederson, J. L., Tressler, C., Mackley, R. D., & Mitchell, K. J. (2015). Rock strength along a fluvial transect of the Colorado Plateau – quantifying a fundamental control on geomorphology. *Earth and Planetary Science Letters*, v. *429*, p. 90–100. https://doi.org/10.1016/j.epsl.2015.07.042.

Burbank, D. W., & Anderson, R. S. (2011). *TECTONIC GEOMORPHOLOGY*.

Cargill, J. S., and A. Shakoor (1990). Evaluation of empirical methods for measuring the uniaxial compressive strength of rock, *Int. J. Rock Mech. Min Sci. & Geomech. Abstr.*, v. 27(6), p. 495-503, doi:10.1016/0148-9062(90)91001-n.

Carson, M.A., (1984). Observations on the meandering-braided river transition, the Canterbury Plains. *New Zealand: Part One: New Zealand Geographer*, v. 40, p.12-19, doi:10.1111/j.1745-7939.1984.tb01477.x.

Carver, G.A., Burke, R.M., and Kelsey, H.M., (1985). Quaternary deformation studies in the region of the Mendocino Triple Junction, in Technical summaries. *National Earthquake Hazard Reduction Program: U.S. Geological Survey Open-File Report*, v. 86-31, p. 58-62.

Collins, B.D., Montgomery, D.R., Schanz, S.A., Larsen, I.J., (2016). Rates and mechanisms of bedrock incision and strath terrace formation in a forested catchment, Cascade Range, Washington. *Geol. Soc. Am. Bull*. https://doi.org/10.1130/B31340.1.

Finnegan, N.J., Dietrich, W.E., (2011). Episodic bedrock strath terrace formation due to meander migration and cutoff. *Geology*, v. 39, p. 143–146. https://doi.org/10.1130/G31716.1.

Finnegan, N.J., Balco, G., (2013). Sediment supply, base level, braiding, and bedrock river terrace formation: Arroyo Seco, California, USA. *Geol. Soc. Am. Bull*. v. 125, p. 1114–1124. https://doi.org/10.1130/B30727.1.

Goudie, A. S. (2006). The Schmidt Hammer in geomorphological research, Prog. *Phys. Geog*., v. 30(6), p. 703-718, *doi:10.1177/0309133306071954.*

Gunckel, S. L., Jones, K. K., & Jacobs, S. E. (2009). Spawning Distribution and Habitat Use of Adult Pacific and Western Brook Lampreys in Smith River, Oregon.

Hance, D. J., Ganio, L. M., Burnett, K. M., & Ebersole, J. L. (2016). Basin-Scale Variation in the Spatial Pattern of Fall Movement of Juvenile Coho Salmon in the West Fork Smith River, Oregon. *Transactions of the American Fisheries Society*, v. *145*(5), p. 1018–1034. https://doi.org/10.1080/00028487.2016.1194892.

Hancock, G. S., and Anderson, R. S., (2002). Numerical modeling of fluvial strath-terrace formation in response to oscillating climate. *Geological Society of American Bulletin*, v. 144, p. 1131-1142.

Hooke, J. M. (2013). 9.16 River Meandering. *In Treatise on Geomorphology* (p. 260–288). Elsevier. https://doi.org/10.1016/B978-0-12-374739-6.00241-4.

Howard, A. D., & Kerby, G. (1983). Channel changes in badlands. *Geological Society of America Bulletin*, v. 94(6), p. 739-752.
https://doi.org/10.1130/0016-7606(1983)94<739:CCIB>2.0.CO;2.

Howard, A. D., & Knutson, T. R. (1984). Sufficient conditions for river meandering: A simulation approach. *Water Resources Research*, v. *20*(11), p. 1659–1667. https://doi.org/10.1029/WR020i011p01659.

Inoue, T., Yamaguchi, S., & Nelson, J. M. (2017). The effect of wet-dry weathering on the rate of bedrock river channel erosion by saltating gravel. *Geomorphology*, v. *285*, p. 152–161. https://doi.org/10.1016/j.geomorph.2017.02.018.

Johnson, K.N., Finnegan, N.J., (2015). A lithologic control on active meandering in bedrock channels. *Geol. Soc. Am. Bull*. v. 127, p. 1766–1776. https://doi.org/10.1130/B31184.1.

kelsey, H.M., (1990). Late Quaternary deformation of marine terraces on the Cascadia subduction zone near Cape Blanco: Tectonics, v. 9, p. 983-1014.

Kelsey, H. M., & Bockheim, J. G. (1994). Coastal landscape evolution as a function of eustasy and surface uplift rate, Cascadia margin, southern Oregon. *Geological Society of America*

Bulletin, v. *106*(6), p. 840–854. https://doi.org/10.1130/0016-7606(1994)106<0840:CLEAAF>2.3.CO;2.

Kelsey, H.M., Engebretson, D.C., Mitchell, C.E., Ticknor, R., (1994). Topographic form of the Coast Ranges of the Cascadia margin in relation to coastal uplift rates and plate subduction. *Journal of Geophysical Research*, v. 99, p. 12245-12255.

Kobor, J. S., & Roering, J. J. (2004). Systematic variation of bedrock channel gradients in the central Oregon Coast Range: Implications for rock uplift and shallow landsliding. *Geomorphology*, v. *62*(3–4), p. 239–256. https://doi.org/10.1016/j.geomorph.2004.02.013.

Kumar, R., and S. K. Ghosh (1991), Sedimentological Studies of the Upper Siwalik Boulder Conglomerate Formation, Mohand Area, District Saharampur, U. P, J, *Himal. Geol*., v. 2, p. 159-167.

Kumar, R. (1993). Coalescence megafan: Multistorey sandstone complex of the late-orogenic (Mio-Pliocene) sub-Himalayan belt, Dehra Dun, India. *Sedimentary Geology*, v. *85*(1–4), p. 327–337. https://doi.org/10.1016/0037-0738(93)90091-I.

Mason, J., & Mohrig, D. (2019). Differential bank migration and the maintenance of channel width in meandering river bends. *Geology*, v. *47*(12), p. 1136–1140. https://doi.org/10.1130/G46651.1.

McInelly, G.W., and Kelsey, H. M., (1990). Late Quaternary tectonic deformation in the Cape Arago-Bandon region of coastal Oregon as deduced from wave-cut platforms. *Journal of Geophysical Research*, v. 95, p. 6699-6713.

McNeill, L.C., Goldfinger, C., Kulm, L.D., Yeats, R.S., (2000). Tectonics of the Neogene Cascadia forearc basin: investigations of a deformed late Miocene unconformity. *Geological Society of America Bulletin*, v. 112, p. 1209-1224.

Miller, R. R. (2010). Is the past present? Historical splash-dam mapping and stream disturbance detection in the Oregon Coastal Province.

Mitchell, C.E., Vincent, P., Weldon II, R. J., Richards, M.A., (1994). Present-day vertical deformation of the Cascadia margin, Pacific Northwest, United States. *Journal of Geophysical Research* v. 99 (B6), p. 12257-12277.

Mitchell, N. A., & Yanites, B. J. (2021). Bedrock River Erosion through Dipping Layered Rocks: QuantifyingErodibility through Kinematic Wave Speed [Preprint]. *Physical: Geomorphology (including all aspects of fluvial, coastal, aeolian, hillslope and glacial geomorphology)*. https://doi.org/10.5194/esurf-2021-3.

Montgomery, D. R. (2004). Observations on the role of lithology in strath terrace formation and bedrock channel width. *American Journal of Science*, v. *304*(5), p.454–476. https://doi.org/10.2475/ajs.304.5.454.

Muhs, D. R., Rockwell, T. K., and Kennedy, G. L., (1992). Late Quaternary uplift rates of marine terraces on the Pacific coast of North America, southern Oregon to Baja California Sur: Quaternary International, v. 15/16, p. 121-133.

Niem, A.R., and Niem, W., (1990) Geology and oil, gas, and coal resources, southern Tyee Basin, Southern Tyee Basin, southern Coast Range, Oregon: Portland, Oreg., Oregon Dept. of Geology and Mineral Industries Open-Fire Report O-89-3, scale 1: 125,000.

O'Connor, J.E., Mangano, J.F., Anderson, S.W., Wallick, J.R., Jones, K.L., Keith, M.K., (2014). Geologic and physiographic controls on bed-material yield, transport, and channel morphology for alluvial and bedrock rivers, western Oregon. *Geol. Soc. Am. Bull*. B30831.1. https://doi.org/10.1130/B30831.1.

Personius, S.F., Kelsey, H.M., Grabau, P.C., (1993). Evidence for regional stream aggradation in the Central Oregon Coast Range during the Pleistocene-Holocene transition. *Quat. Res*. v. 40, p. 297–308. https://doi.org/10.1006/qres.1993.1083.

Personius, S.F., (1993) Age and origin of fluvial terraces in the central Coastal Range, western Oregon. *U.S. Geological Survey Bulletin*. v. 2038, 56., 4pl.

Pazzaglia, F. (2013). 9.22 Fluvial Terraces. *In Treatise on Geomorphology*, v. 9, p. 379-412. https://doi.org/10.1016/B978-0-12-374739-6.00248-7.

Reneau, S. L., and Dietrich, W. E., (1991). Erosion rates in the southern Oregon Coast Range: Evidence for an equilbrium between hillslope erosion and sediment yield. *Earth Surface Processes and Landforms*, v. 16, p. 307-322.

Ticknor, R. L., (1992). Late Quaternary crustal deformation on the central Oregon coast as deduced from uplifted wave-cut plateforms [M.S. thesis]: Bellingham, Washington, Western Washington University, p. 60.

Schanz, S. A., & Montgomery, D. R. (2016). Lithologic controls on valley width and strath terrace formation. *Geomorphology*, v. *258*, p. 58–68. https://doi.org/10.1016/j.geomorph.2016.01.015.

Selby, M. J. (1993), Hillslope Materials and Processes, *Oxford University Press*, Oxford, UK, 2nd ed.

Seminara, G. (2006). Meanders. *Journal of Fluid Mechanics*, v. *554*(1), p. 271. https://doi.org/10.1017/S0022112006008925.

Sklar, L.S., Dietrich, W.E., (2004). A mechanistic model for river incision into bedrock by saltating bed load. *Water Resour. Res*, v. 40. https://doi.org/10.1029/2003WR002496.

SRWA, (1997). Smith River Watershed Analysis. Prepared by: Siuslaw National Forest and BLM Coos Bay. US Forest Service and Bureau of Land Management.

Stark, C. P., Barbour, J. R., Hayakawa, Y. S., Hattanji, T., Hovius, N., Chen, H., Lin, C.-W., Horng, M.-J., Xu, K.-Q., & Fukahata, Y. (2010). The Climatic Signature of Incised River Meanders. *Science*, v. *327*(5972), p. 1497–1501. https://doi.org/10.1126/science.1184406.

Walker, G. W., Duncan, R. A., (1989). Geologic Map of the Salem 1 degrees by 2 degrees Quadrangle, Western Oregon. Miscellaneous Investigations Series-U.S. *Geological Survey*, v. I-1893. Reston, VA.

Walker, G.W., MacLeod, N.S., (1991). Geologic map of Oregon. Special map U.S. *Geological Survey*, Reston, VA.

West, D. O., McCrumb, D.R., (1988). Coastline uplift in Oregon and Washington and the nature of Cascadia subduction-zone tectonics. *Geology*, v. 16, p. 169-172.

Whipple, K. X., Hancock, G. S., & Anderson, R. S. (2000). River incision into bedrock: Mechanics and relative efficacy of plucking, abrasion, and cavitation. *Geological Society of America Bulletin*, 14.

Whipple, K. X., & Tucker, G. E. (1999). Dynamics of the stream-power river incision model: Implications for height limits of mountain ranges, landscape response timescales, and research needs. *Journal of Geophysical Research: Solid Earth*, v. *104*(B8), p. 17661–17674. https://doi.org/10.1029/1999JB900120.

Wohl, E. (2015). Particle dynamics: The continuum of bedrock to alluvial river segments. *Geomorphology*, v. *241*, p. 192–208. https://doi.org/10.1016/j.geomorph.2015.04.014.

Yanites, B. J. (2018). The Dynamics of Channel Slope, Width, and Sediment in Actively Eroding Bedrock River Systems. *Journal of Geophysical Research: Earth Surface*, v. *123*(7), p. 1504–1527. https://doi.org/10.1029/2017JF004405.

Yanites, B. J., Tucker, G. E., Mueller, K. J., Chen, Y.-G., Wilcox, T., Huang, S.-Y., & Shi, K.-W. (2010). Incision and channel morphology across active structures along the Peikang River, central Taiwan: Implications for the importance of channel width. *Geological Society of America Bulletin*, v. *122*(7–8), p. 1192–1208. https://doi.org/10.1130/B30035.1.